Bulletin of the Earthquake
Research Institute
Vol. 40 (1962), pp. 187-259

8. *Modifications of Seismic Waves in Superficial Soil Layers as Verified by Comparative Observations on and beneath the Surface.*

By Etsuzo Shima,

Earthquake Research Institute.

(Read Oct. 27, 1959; June 27 and Nov. 28, 1961.—Received March 31, 1962.)

CONTENTS

Preface

Many seismologists throughout the world are keenly interested of late in the study of the mechanisms and magnitudes of earthquakes. Both of these problems must basically have recourse to a knowledge of the motion imparted to the seismic waves at the hypocentral region of an earthquake. In most of the current studies it is implicitly assumed that the modification of earthquake waves on the way from the hypocentre to an observation point is not of so marked a degree as to be taken into account. However, it is a well-known fact that the seismic intensity on different grounds in the same vicinity differs so remarkably as to alter the degree of damage several times over. In view of these experiences quantitative study on the modification of seismic waves is no less important in pure seismology than in engineering seismology.

From the earthquake engineering point of view, the problem has been taken up for about 40 years. The theory of the refraction of elastic waves taught us that the softer the second medium into which the elastic wave is refracted from the hard first medium, the larger becomes the refracted wave. But aftershock observations of the 1923 earthquake in Tokyo and Kamakura revealed to us that enhancements of amplitudes of the same earthquake on different neighbouring grounds are not in a constant ratio, but the ratio varies with the periods of the earthquake motions.

An explanation of this phenomenon by the resonance effect of the surface layers was proposed and stimulated study on the possibility as well as the nature of these vibration characteristics of soil layers from the theoretical and observational sides.

Much light has been thrown on the problem by the above-mentioned studies but still there is left something to be clarified. The present paper is concerned with the last point. In the following an effort to verify the above-mentioned modifications of seismic waves in the superficial soil layers has been made by comparative observations on and beneath the surface of the ground. For this purpose a special seismometer to be installed underground in a bore-hole was first made and

observations by means of sets of the same instruments were carried out. Besides the analyses of the seismograms thus observed, analyses of microtremors observed on the ground were also made as another approach to the elucidation of the problem.

Thus in Part 1 in this paper a description of a bore-hole seismometer is given, and in Part 2 an automatic correlator, to be used in the analyses of microtremors, is described. In the last section Part 3, analyses of seismograms obtained from simultaneous observations of earthquake motions on and beneath the surface of the ground are described and compared with the facts revealed by means of the correlator from the analyses of microtremors.

Before entering into the main subject, a historical review of the related studies will be given to clarify the problem.

With regard to the theoretical studies, K. Sezawa[1], G. Nishimura[2] and K. Kanai[3] began energetic persistent study on the present problem in 1930, with the result that various aspect were thereby clarified. They investigated cases when disturbances of the shock type[4] and of the harmonic type of finite extent[5] are transmitted from the subjacent semi-infinite medium normally upwards to the overlying stratum or strata.

Through their studies, it was revealed that, in the case of a single layer, the displacement of the ground surface and the reflected waves into the subjacent medium show a periodicity in shock type waves when the length of the travelling disturbance in the stratum is short as compared with the thickness of that surface stratum. But, when the length is comparatively long, there is no sign of apparent periodicity in the motions on surface and reflected waves. And also in the case of an incidence of a harmonic wave of a finite extent free oscillation is never excited in any stratum.

They reached a similar conclusion in the case where there are two surface strata[6]. When the harmonic type wave of a finite extent is normally incident, the surface vibration consists of a wave train which repeats itself with a gradually diminishing amplitude. And the periodicity which we observe is the periodicity contained in the incident wave. In the case of an incidence of a shock type wave, repetition of similar wave

1) K. SEZAWA, *Bull. Earthq. Res. Inst.*, **8** (1930), 1.
2) K. SEZAWA, and G. NISHIMURA, *Bull. Earthq. Res. Inst.*, **8** (1930), 321.
3) K. SEZAWA and K. KANAI, *Bull. Earthq. Res. Inst.*, **10** (1932), 273.
4) *loc. cit.*, 2).
5) *loc. cit.*, 3).
6) *loc. cit.*, 3).

trains is observed so that we might call the periodic recurrence time of the vibration as the proper period of the strata.

Briefly, K. Sezawa and K. Kanai came to the conclusion that, in the case of a harmonic type of a finite extent, the free oscillation of the layer can not be excited except when the products of elastic modulus and density in respective media differ appreciably. G. Nishimura and T. Takayama[7] solved more practical cases than those of Sezawa and Kanai. Namely, they studied the vibrations due to obliquely incident waves. And they confirmed that there exist proper periods of vibration in the surface layer.

From seismometrical observations it was known at that time that there are some differences between seismograms observed at stations having different topographical or subsoil conditions. J. Milne[8] was the first to attempt this type of study. He compared a seismogram obtained by a seismometer which was set at the bottom of a 10′ deep well with one obtained from a seismometer on the ground 30′ distant. Then, S. Sekiya and F. Omori[9] also carried out the same experiment on the campus of the University of Tokyo, setting a seismometer in the cellar 18′ deep. N. Nasu[10] observed numerous aftershocks of the Great Kwanto Earthquake at many temporary stations in Tokyo. And comparing them with those of Hongo, he found that amplitude-ratio becomes large at a period which is proper to the station. S. T. Nakamura[11] performed observations in and out of a tunnel near Atami. N. Nasu[12] also made comparative observations at the Tanna Basin and in Tanna Tunnel 160 m below the surface observing point.

K. Suyehiro[13], on the other hand, invented a model of a seismic-vibration analyser, and used it for comparative studies.

Following these studies the predominating periods of the seismic waves were observed at various temporary stations by many investigators.

M. Ishimoto[14] performed comparative observations at Tokyo and at Yokohama, using his accelerometers, and determined the proper pre-

7) G. NISHIMURA and T. TAKAYAMA, *Bull. Earthq. Res. Inst.*, **15** (1937), 394.
8) J. MILNE, *Trans. Seism. Soc. Japan*, **10** (1887), 1.
9) S. SEKIYA and F. OMORI, *Trans. Seism. Soc. Japan*, **16** (1892).
10) N. NASU, *Rep. Imp. Earthq. Inv. Comm.*, **100** A, 313.
11) S. T. NAKAMURA, *Proc. Physico-Mathem. Soc. Japan*, **7** (1925) 127.
12) N. NASU, *Bull. Earthq. Res. Inst.*, **9** (1931), 454.
13) K. SUYEHIRO, *Bull. Earthq. Res. Inst.*, **1** (1926), 59; *ibid.*, **7** (1926), 467.
14) M. ISHIMOTO, *Bull. Earthq. Res. Inst.*, **9** (1931), 316; *ibid.*, **9** (1931), 473; *ibid.*, **10** (1932), 171; *ibid.*, **12** (1934), 234; *ibid.*, **14** (1936), 240; *ibid.*, **15** (1937). 536.

dominant period at each place. He also found a close relation between the thickness of the subsoil and the proper periods. T. Saita and M. Suzuki[15] compared earthquake accelerations of the surface with accelerations at points 30′ and 68′ below the surface at Marunouchi. They set the accelerometers in a well. W. Inouye[16] observed amplitudes at Komaba both in a cellar 9 m deep and in an observation room on the surface.

Their explanations concerning the oscillations of a surface layer of subsoil involved the assumption that the surface layer may be treated as a pendulum which gives no reaction to the underlying medium, so that the motion on the surface has no relation to the vibration in the subjacent medium. This way of thinking is definitely irrelevant according to the mathematical theory worked out by K. Sezawa[17] and G. Nishimura[18]. Namely, the mode of resonant oscillation is not always coincident with the mode of the free oscillation of the pendulum which is considered as a model. But, the fact that the predominating period of the subsoil is proportional to the thickness of the alluvial formation is powerful evidence supporting the hypothesis of proper oscillation.

Afterwards, based on comparative study of seismograms, R. Takahasi and K. Hirano[19] proved both by theory and experiment the phenomena of predominating waves considering the multiple reflections of the waves in the surface layer.

K. Kanai and others[20] have compared the seismograms obtained at the gallery of the Hitachi Mine. The depths of the stations are 0, 150, 300 and 450 m respectively. And the results supported the proper oscillation hypothesis.

Meanwhile, on the theoretical side, K. Kanai[21] succeeded to Sezawa's studies, and he explained the predominant periods of the strata by the multiple reflections of the seismic waves in the strata. In his study

15) T. Saita and M. Suzuki, *Bull. Earthq. Res. Inst.*, **12** (1934), 517.

16) W. Inouye, *Bull. Earthq. Res. Inst.*, **12** (1934), 712.

17) *loc. cit.*, 1).
K. Sezawa and K. Kanai, *Bull. Earthq. Res. Inst.*, **13** (1935), 251.

18) *loc. cit.*, 7).

19) R. Takahasi and K. Hirano, *Bull. Earthq. Res. Inst.*, **19** (1941), 534.

20) K. Kanai and T. Tanaka, *Bull. Earthq. Res. Inst.*, **29** (1951), 107.

21) K. Kanai, *Bull. Earthq. Res. Inst.*, **28** (1950), 31; *ibid.*, **30** (1952), 32; *ibid.*, **31** (1953), 210.
K. Kanai and S. Yoshizawa, *Bull. Earthq. Res. Inst.*, **31** (1953), 275; *ibid.*, **34** (1956), 167.
K. Kanai, *Bull. Earthq. Res. Inst.*, **35** (1957), 309; 457.

the effect of the solid viscosity of a surface layer was also taken into consideration. For the purpose of practical applications he studied the case of three superficial layers.

As for seismometrical studies, F. Omori[22] found that waves with periods peculiar to the observation station and related to the subsoil condition, predominate not only in disturbances due to earthquake waves but also in microtremors. Although it is a very difficult matter to analyse such complicated waves quantitatively, we fortunately have Ishimoto's excellent paper[23], which opened the way for an approach to the solution.

Since 1954, K. Kanai and others[24] have taken up again the problem of microtremors. They have compared the frequency-period curves derived from the numerous records of microtremors observed at various places in Japan. For their view, the method of analysis is as follows. By taking any two minutes portion from records of microtremors, the zero-crossing intervals are measured. This interval is doubled and it is considered as a period. Then, taking the period on the abscissa and the number of waves of each period on the ordinate, the curve of the frequency-period[25] is drown. Kanai found that the frequency-period curves thus derived from the records of microtremors resemble markedly those derived from earthquake observations. Comparing with the other information related to soil conditions near the observation site, Kanai could derive a convenient method based on microtremor observations for classifying the subsoil.

On the other hand, K. Aki[26] and K. Akamatu[27] took up the study of microtremors at almost the same time, and introduced the correlogram analysis into their analyses. Some of the characteristics of microtremors were thus clarified. And Akamatu recognized some evidence on the existence of the proper period, although Aki's[28] result of a correlogram analysis had been negative on the same point.

---

22) F. OMORI, *Bull. Earthq. Inv. Comm.*, **2** (1908), 1.

23) M. ISHIMOTO, *Bull. Earthq. Res. Inst.*, **15** (1937), 697.

24) K. KANAI *et al.*, *Bull. Earthq. Res. Inst.*, **32** (1954), 199; *ibid.*, **33** (1955), 492; *ibid.*, **35** (1957), 135; 147; 163; 181; 191.

25) K. KANAI *et al.*, *ibid.*, **32** (1954), 201.

26) K. AKI, *Bull. Earthq. Res. Inst.* **25** (1957), 415.

27) K. AKAMATU, *Zisin* [ii] **9** (1956), 22.

28) K. AKI, *Zisin* [ii] **8** (1955), 99.

Part 1

The Bore-hole Seismometer

1. Introduction

Needless to say, deep underground observation of earthquake motions is indispensable to the crucial study of the frequency characteristics of ground vibrations. Several attempts of such observations have been made by former investigators, like Saita[29] and Inouye[30]. However, as they utilized mechanical recording instruments, many restrictions troubled them. For instance, Saita and Suzuki had to use a big well to install the acceleration seismographs at depths in the ground. And under such circumstances, we have no evidence that the characteristics of the near-by subsoil did not differ. If they had had an electro-magnetic bore-hole seismometer, and could set it at the bottom of a small bore-hole, the above-mentioned circumstances and many other restrictions could have been eliminated. Besides this, remote operation of the seismometer would have reduced the operational problems. Unfortunately, the instrument relevant for this purpose did not exist at that time. Of course in later times, in the field of seismic prospecting, many bore-hole geophones were introduced. However, the natural frequencies of these geophones were too high to be useful for our present purpose.

In the following, we will outline a bore-hole seismometer specially designed for observation of earthquake motions in the depths of the ground. To the best of our knowledge, this seismometer is the first one ever designed for this purpose. The frequency characteristics of this seismometer are proportional to the ground acceleration in the frequency range from 1 to 20 cycles per second. We coupled this seismometer (natural period $=1.8$ sec), and the overall frequency characteristics of this seismograph are proportional to the ground displacement in the abovementioned frequency range.

2. Principles of design

Two methods can be considered, at least theoretically, for ascertaining the displacement of earth movement in a wide frequency range

29) *loc. cit.*, 15).
30) *loc. cit.*, 16).

with the electromagnetic seismometer. The seismometer we are concerned with here is a moving-coil type which has an excellent linear response to earth movement, and is easy to design.

The first method is as follows. Design a low damping seismometer (optimum would be $h \approx 0.6$). Then the pendulum of the seismometer responds to the earth movement in proportion to its displacement at a frequency higher than the natural frequency of the seismometer. Now the output voltage is proportional to the velocity of the earth movement. Couple this seismometer to a galvanometer which is heavily damped and has a higher natural frequency than that of the seismometer. The sensitivity of such a galvanometer, when the input current is of a constant magnitude, attenuates in proportion to a frequency near the natural frequency of the galvanometer. In other words, the galvanometer acts as an integrator. Through the combination of the above seismometer and galvanometer we have a seismogram which is proportional to the earth movement. The above-mentioned results are verified as follows.

At first, let us study the equivalent network of the galvanometer. Using the electrical mechanical analogy, which we have already applied once to our discussion of a seismometer[31], we easily reach the result shown in Fig. 1, in which, r_g is the internal resistance of the coil, l_g

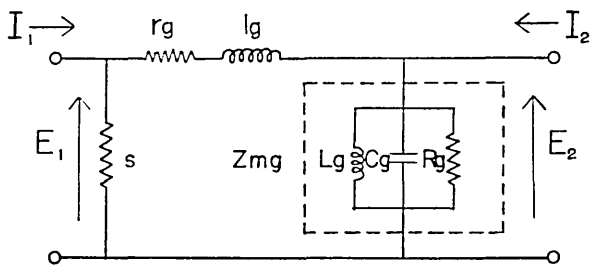

Fig. 1. Equivalent network of the galvanometer

is the sum of self inductance, hysteresis and eddy current losses; and s is the shunt resistance. Z_{mg} is the motional impedance of the galvanometer and is expressed as the parallel connection of the capacitance C_g, the resistance R_g and the inductance L_g. These electrical quantities have the following relations with the mechanical quantities through the voltage sensitivity A_g of the galvanometer. Namely, $C_g = I_g/A_g^2$, $R_g = A_g^2/b_g$ and $L_g = A_g^2/U_g$. Where I_g, b_g and U_g are the moment of inertia, the damping constant and the restoring constant of the galvanometer re-

31) E. SHIMA, *Bull. Earthq. Res. Inst.*, **38** (1960), 29.

spectively. The mechanical entities and their electrical equivalents are listed in Table 1.

Table 1.

Mechanical element	Symbol used	Electrical element	Symbol used
Torque	F_R	Current	I
Angular Velocity	ω	Voltage	E
Moment of Inertia	I_g	Capacitance	C_g
Rotational Compliance	$1/U_g$	Inductance	L_g
Rotational Resistance	b_g	Conductance	$1/R_g$
Angular Displacement	φ		$\int Edt$

Let y be the response on the recording paper by the rotation of the galvanometer, we have,

$$y=2l\varphi=\frac{2l}{A_g}\int E_2 dt\,, \tag{1}$$

where l is the optical lever of the galvanometer. Generally, the magnitude of resistance R_g is very large. This fact is known if we observe the slow damping of the free oscillation of the galvanometer. And l_g is negligibly small at low frequencies. For the sake of simplicity we overlook the above two quantities. Now, if we observe the equivalent circuit from a mechanical side, the galvanometer is expressed by the parallel connection of (r_g+s), L_g and C_g. So, from the mechanical point of view, the natural frequency n and the damping coefficient ε and $h=\varepsilon/n$ are expressed as follows:

$$\left.\begin{aligned} n^2&=\frac{1}{L_gC_g}\\ \varepsilon&=\frac{1}{2(r_g+s)C_g}\end{aligned}\right\}, \tag{2}$$

and

$$h=\frac{1}{2(r_g+s)}\sqrt{\frac{L_g}{C_g}}\,. \tag{3}$$

It is clear from Equation (3) that, in the case when $s\to\infty$, h becomes very small. In the case of an open circuit, s is considered to be infinitesimal. Now we have,

$$E_2=\frac{I_1 s\dfrac{j\omega L_g}{1-\omega^2 L_g C_g}}{(s+r_g)+\dfrac{j\omega L_g}{1-\omega^2 L_g C_g}}. \tag{4}$$

So, if $\omega^2\approx 1/L_gC_g$, $h\gg 1$

$$E_2\doteqdot I_1 s=const\,, \tag{4'}$$

$$\therefore\quad y\propto\int I_1\, s\, dt\,. \tag{5}$$

Thus the integrating characteristics of the galvanometer are proved.

However, it is necessary for this purpose to design a seismometer which has a longer natural period than the earthquake period we are to observe. Our purpose is to set a seismometer in a bore-hole, so we are concerned as to whether or not a long period seismometer can be set satisfactorily in it[32]. Moreover, as a long period seismometer cannot withstand violent handling, it may be broken during the setting.

Now we outline the second method. We design a heavily damped seismometer so that the pendulum of the seismometer responds to the velocity of the earth movement. Then we have an output voltage which is proportional to the ground acceleration. Couple this to a galvanometer which has a longer natural period than that of the seismometer. The damping of the galvanometer is recommended to have a value near $h=0.6$. The sensitivity of such a galvanometer in a frequency range higher than that of the galvanometer attenuates in proportion to ω^2. In other words, the galvanometer acts as a twice-integrator. Thus we have seismograms which are proportional to the ground displacement.

The above-mentioned results are verified as follows. Under the conditions $\omega^2\gg 1/L_gC_g$ and $\omega\gg 1/C_g(s+r_g)$, Equation (4) becomes,

$$E_2\doteqdot\frac{I_1 s}{j\omega C_g(s+r_g)}\,, \tag{4''}$$

$$\therefore\quad y\propto\int\frac{I_1}{j\omega C_g}dt\propto\iint\frac{I_1}{C_g}dt\,dt\,, \tag{5'}$$

which is to be proved.

A seismometer designed along these lines can be used as an electro-

32) After completing the construction of our seismometer, K. Kanai and T. Tanaka designed a seismometer free from these difficulties.

K. KANAI and T. TANAKA, *Bull. Earthq. Res. Inst.*, **36** (1958), 359.

magnetic acceleration seismograph if we couple it to a galvanometer which has a much higher natural frequency than that of the seismometer. Namely, if $\omega \ll (s+r_g)/L_g$ and $\omega^2 \ll L_g C_g$, Equation (4) becomes.

$$E_2 \doteqdot \frac{j\omega L_g I_1 s}{s+r_g}\,, \tag{4'''}$$

$$\therefore \quad y \propto L_g I_1\,. \tag{5''}$$

The above-mentioned accelerometer is perhaps useful for persons in the engineering field. And this is the reason for our adopting the latter type of seismometer.

3. Actual design

Fig. 2 is a schematic view of the 3-component bore-hole seismometer. In designing the magnetic circuit, which is the most important part of the seismometer, we were obliged to reduce its size because it was necessary to set the 3-component seismometer, one vertical and two horizontal, in a bore-hole of small diameter. For this purpose, we used the smallest cylinder type permanent magnet MK-5[33]. We have already reported examples of magnetic circuit designs of this type[34].

During the designing, a special care was paid to make the voltage sensitivity insensible to the inclination of the seismometer. In Fig. 3, an example is given showing how the voltage sensitivity of a seismometer changes its magnitude according to the deflection of the coil from the centre of its equilibrium.

We had to be cautious, fearing that the seismometer would not always be upright in the bore-hole. So bore-hole seismometers have to be stable in their functioning even when they are set slantwise from the vertical to a marked degree. The usual type of seismometer which makes use of a horizontal pendulum is impotent in such circumstances, so we spent much effort in designing the pendulum. Fortunately we found that Willmore suspension[35]—to suspend the mass by 6 slender wires—is very apposite for this purpose. This type of suspension is shown in Fig. 4 as well as in Fig. 2. We find the mass swings inside the cylinder and is suspended by 3 wires. The other 3 wires are also used to suspend the mass from the opposite side.

33) Product of Mitsubishi Kozai Co. Ltd.

34) E. SHIMA, *Bull. Earthq. Res. Inst.*, **38** (1960), 545.

35) P. L. WILLMORE, *Monthly Not. Roy. Astr. Soc., Geophys. Suppl.*, **6** (1950), 129.

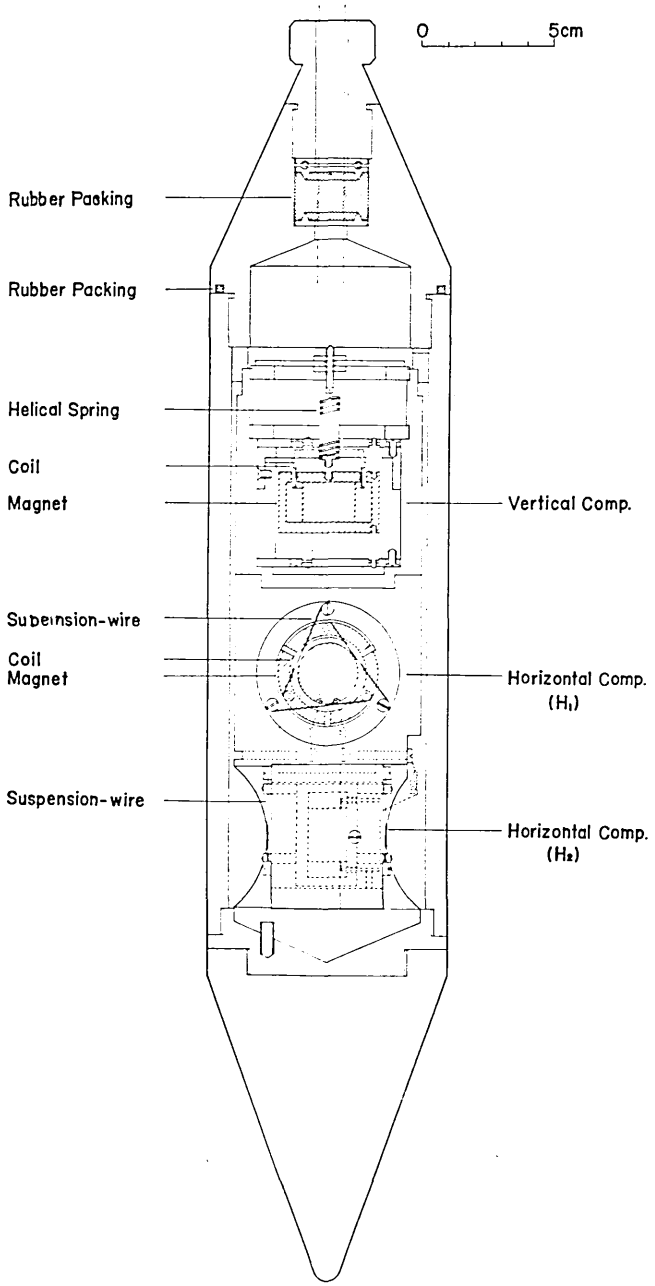

Fig. 2. Schematic view of the three-component bore-hole seismometer.

For the preliminary test, we examined how the period of the pendulum is influenced by the inclination of the pendulum as well as the rotation as a whole around the axis of the cylindrical mass. The results are tabulated in Tables 2 and 3. α is the angle between the wire of the left side and the vertical line as shown in Fig. 4. And β in Table 3 is the angle of inclination of the mass from the vertical line.

The results of Table 3 shows that, so far as our experimental accuracy and our need in the accuracy is concerned, we can assume as a first approximation, that T is insensible to the changes in β as well as α. From

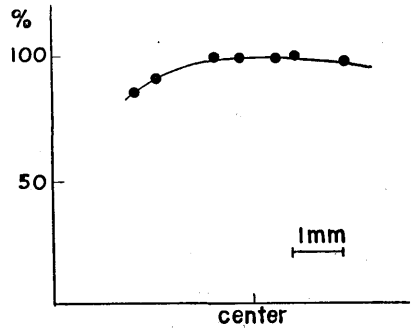

Fig. 3. Variation of the magnitude of voltage sensitivity of a seismometer according to the deflection of the coil from the centre of its equilibrium.

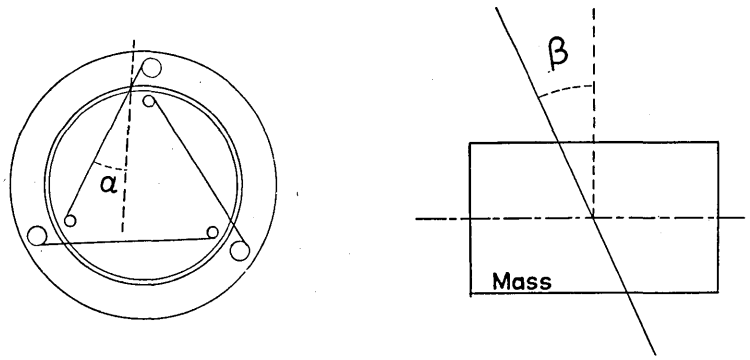

Fig. 4.

Table 2.

α degree	sec
0°	0.207
30	0.207
60	0.208

Table 3.

β degree	sec
0°	0.207
2.5	0.208
6.4	0.210
9.0	0.204

the above results we came to the conclusion that Willmore suspension is apposite for our purpose. In an experiment β could be increased up to 17°, and above this angle the pendulum does not swing because of

knocking against the outer frame. If we set the seismometer in a bore-hole, 6 inches in diameter, β does not exceed 10° even in the worst circumstances. So we may say that if we can set the seismometer at the bottom of a bore-hole of such diameter, we can expect its stable function.

The mass of the vertical seismometer is suspended upright by a helical spring, and it controls the period. Willmore suspension was also used in the vertical seismometer to keep the mass in the central axis of the seismometer. Though two horizontal components were assembled in the same frame, the vertical one was made independent, so that it can be taken out of the outside case of the 3-component seismometer, and used separately. The pendulum of the seismometer was damped heavily with silicon oil, the viscosity of which is 15 centistokes. Without the damping oil we could not get the desired damping of the pendulum. It is clear that the effect of electro-magnetic damping is very small, even if the output terminals are short-circuited, h remains near 0.15, because of the large mass and the small voltage sensitivity.

The outer case was first made of aluminum cast. But owing to the pin holes existing in the cast, water sneaked into the case. And so we had to use a brass cylinder. Special attention was paid to the construction of the outlet of the lead wires from the seismometer case. As illustrated in Fig. 2, the cabtyre cord is pressed by rubber-packing so that water can not sneak into the case from this section. It is recommended for this purpose to use cabtyre cord made of rubber.

4. Constants of the seismometer and galvanometer

The constants of the seismometer and the galvanometer are tabulated in Tables 4 and 5. We used the GU-52-B type galvanometer, one of the products of Murayama Electric Co.

Table 4.

Weight of the Mass	M	155 gr
Natural Period	T	0.2 sec
Coefficient of Damping	h	5
Internal Resistance	r_e	90 Ω
Voltage Sensitivity	A	0.10 volt/kine

Table 5.

Natural Period	T_g	1.8 sec
Internal Resistance	r_g	8.6 Ω
External Critical Damping Resistance	r_{cr}	90 Ω
Current Sensitivity	A_{IG}	5.8×10^{-7} amp/cm

5. Frequency characteristics and the calibration of the seismograph

The output voltage of the seismometer is proportional to the acceleration of the ground, because the seismometer is damped heavily so that response of the pendulum is proportional to the ground velocity. In our seismograph the mass is so large that the reaction due to the galvanometer's circuit is negligibly small. So we can obtain the frequency characteristics of the seismograph merely by multiplying each frequency characteristic. The block-diagram of this seismograph is shown in Fig. 5. $i(j\omega)$, $S(j\omega)$, $g(j\omega)$, $f(j\omega)$ and $o(j\omega)$ are the frequency

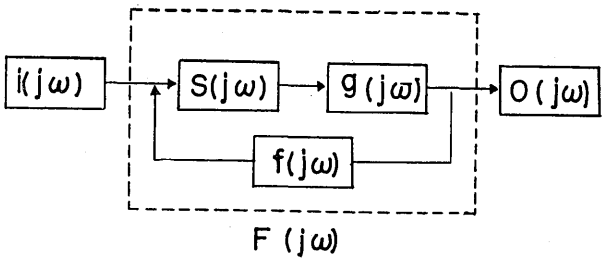

Fig. 5. Block-diagram of the seismograph.

characteristics of the input, seismometer, galvanometer, quantity related to the reaction of the galvanometer and output, respectively. We can obtain them by Fourier transformation as shown in Equation (6).

$$\begin{Bmatrix} i(j\omega) \\ S(j\omega) \\ g(j\omega) \\ f(j\omega) \\ o(j\omega) \\ F(j\omega) \end{Bmatrix} = \int_{-\infty}^{\infty} \begin{Bmatrix} i(t) \\ S(t) \\ g(t) \\ f(t) \\ o(t) \\ F(t) \end{Bmatrix} e^{-j\omega t} dt \,, \tag{6}$$

where $i(t)$ is the time function of the input, and $o(t)$ is the output motion

due to the input i(t). $S(t)$, $g(t)$, $f(t)$, and $F(t)$ are respective impulse responses. $F(j\omega)$ is the over-all frequency characteristics of the seismograph. Strictly speaking, we can easily deduce the following equation from the block diagram shown in Fig. 5.

$$F(j\omega)=\frac{S(j\omega)g(j\omega)}{1-f(j\omega)S(j\omega)g(j\omega)} . \tag{7}$$

However, in our case, the reaction factor $f(j\omega)$ is very slight as mentioned before. So Equation (7) reduces to,

$$F(j\omega)\fallingdotseq S(j\omega)g(j\omega) . \tag{8}$$

The calculated $S(j\omega)$ is shown in Fig. 6. In Fig. 7, the observed $g(j\omega)$ is shown. From these data, we calculated $F(j\omega)$ and it is shown in Fig. 8.

Now referring to Fig. 3, we assume that the voltage sensitivity

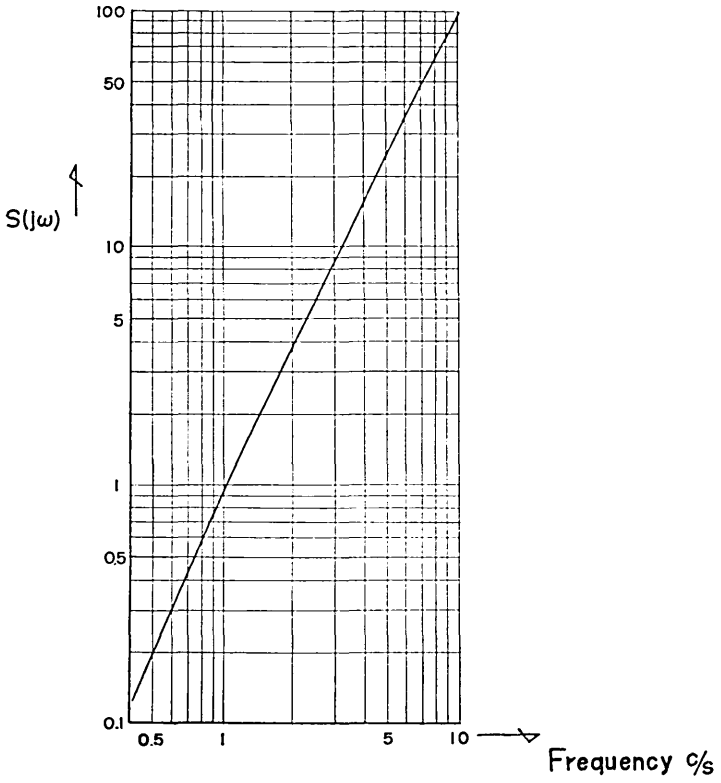

Fig. 6. $S(j\omega)$

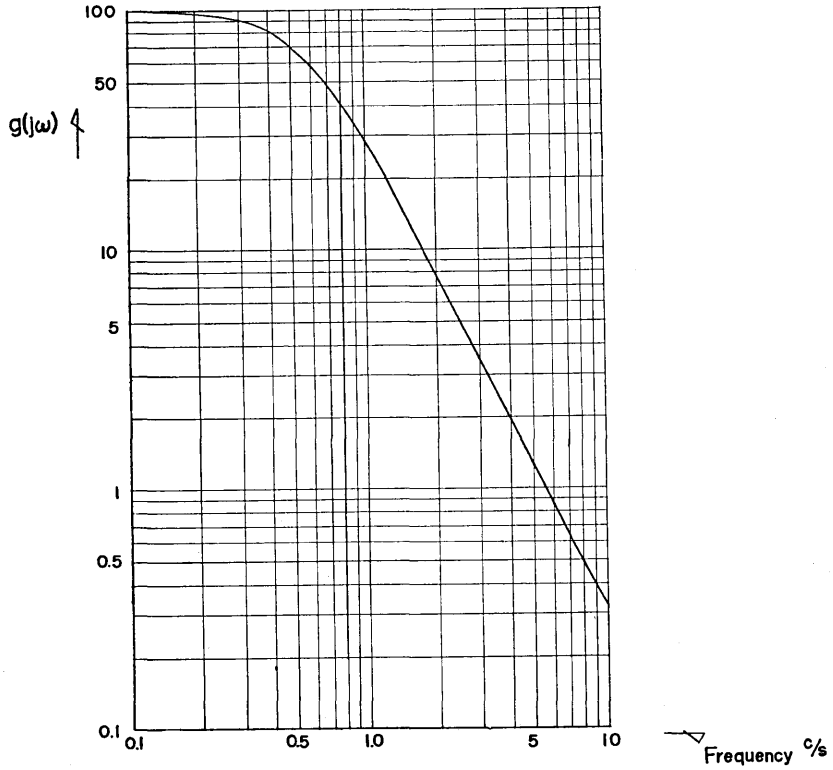

Fig. 7. $g(j\omega)$

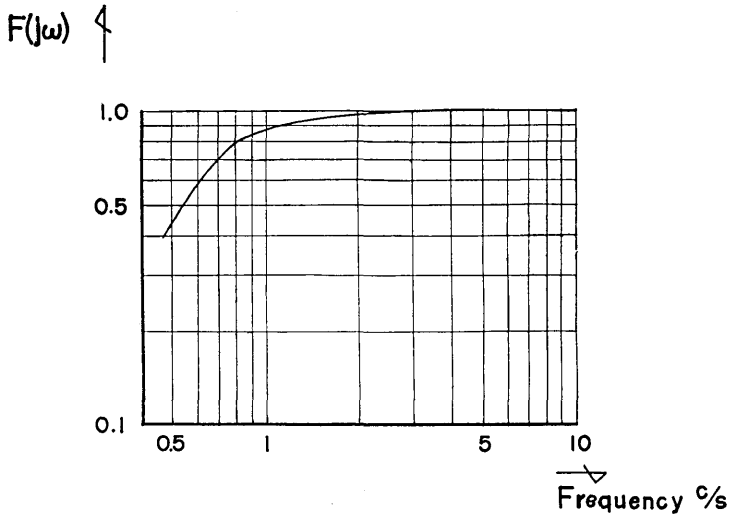

Fig. 8. $F(j\omega)$

does not change with the inclination of the seismometer when it is set at the bottom of a bore-hole. Thus we get the output voltage of the seismometer, near the frequency of its natural frequency, with respect to the unit acceleration as $A/2\varepsilon$ (Volt/gal) or $A/2\varepsilon\,(r_c+r_g)$(Amp/gal). We know the current sensitivity of the galvanometer from observations at each frequency. So we can calculate the deflection y. The sensitivity of the bore-hole seismometer is 320 μV/gal. When we coupled it with the GU-52-B type galvanometer, we could attain a magnification of 80, in the case of a 50 cm optical lever. The optical lever of the GU-52-B type is changeable to that of 100 cm by a simple operation. So the magnification can be doubled in a simple way.

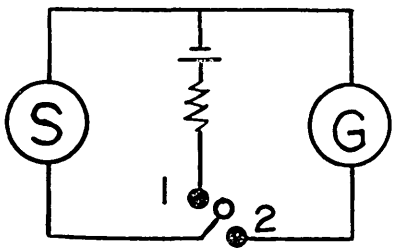

Fig. 9. Simple circuit to check the frequency characteristics of the seismometer.
S: Seismometer, G: Galvanometer.

We felt it necessary to check the frequency characteristics of the seismometer after it had been set at the bottom of the bore-hole. So we made a simple circuit for checking it. The circuit is shown in Fig. 9.

Now let us state the method. First, a switch is set in position 1. Then the current, say i, flows into the seismometer's circuit, and the force f_0 is generated. This force is expressed in terms of the voltage sensitivity or force factor[36] as follows.

$$f_0 = Ai\,. \qquad (9)$$

By this force, the mass of the seismometer is deflected. The deflection

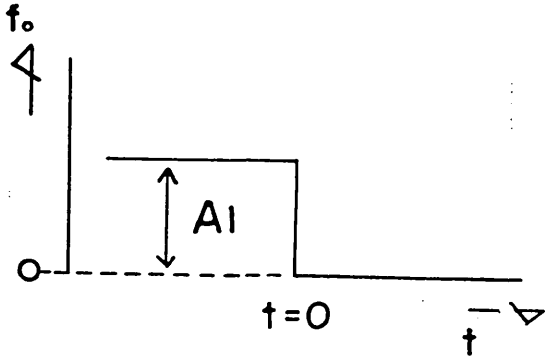

Fig. 10. Step force acting on the seismograph.

36) *loc. cit.*, 31).

of the mass is proportional to the magnitude of the current. Next, we suddenly open the switch and transfer it to position 2. This operation is analogous in applying the step force to the seismograph. Namely, at $t<0$, the force Ai is acting on the seismograph, and at $t=0$, the switch position is changed and the force suddenly becomes zero. Fig. 10 shows this operation.

Let us denote the Fourier transform of the response of the galvanometer in the above case by $R(j\omega)$. We arrive at the following formula, by the multiplication of the Fourier transform of the actual force and the transfer function $F'(j\omega)$ in galvanometric response to the applied force,

$$F'(j\omega)\int_{-\infty}^{\infty} f_0 u(t) e^{-j\omega t}\,dt = R(j\omega)\,, \tag{10}$$

where f_0 is as given in Equation (9) and $u(t)$ is the unit step function defined by the following relations:

$$\begin{aligned} u(t)&=1 \qquad t\geqq 0\,,\\ &=0 \qquad t<0\,. \end{aligned} \tag{11}$$

Substituting Equation (11) into Equation (10), we have.

$$\frac{f_0}{j\omega}F'(j\omega)=R(j\omega)\,, \tag{10'}$$

$$\therefore \quad \frac{j\omega R(j\omega)}{f_0}=F'(j\omega)\,. \tag{10''}$$

The Equation (10″) expresses the frequency characteristics of the seismograph when the unit force in each frequency is applied to the seismograph. Now from Equation (10″), we came to the important conclusion on $F(j\omega)$ defined in the proceeding paragraph as follows:

$$F(j\omega)\propto R(j\omega)\,(j\omega)^3\,. \tag{12}$$

In this method, there is no need to bother with the terms of the reaction of the galvanometer or any other cause because all these effects are automatically included in $R(j\omega)$. This is one of the merits of this method. In Fig. 11, an example of the response of the galvanometer is shown.

Applying the Fourier transformation to this record, we calculated the frequency characteristics $F(j\omega)$, and the result is shown in Fig. 12.

The full-line curve in Fig. 12 is the same with that already shown in Fig. 8. Comparing these results we found a strong agreement between them.

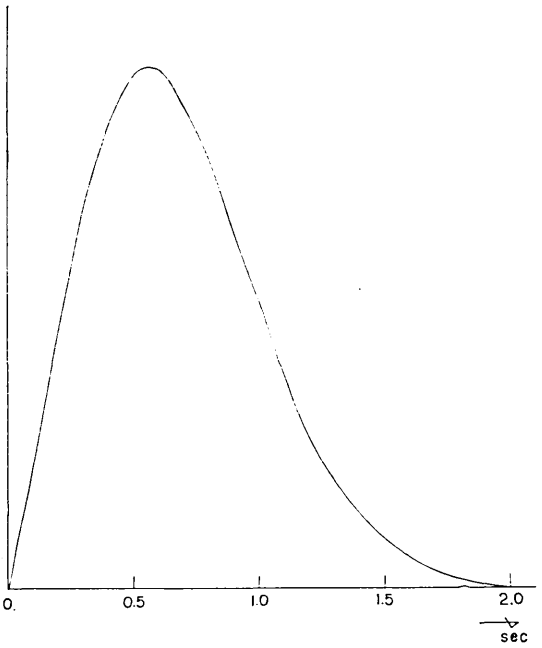

Fig. 11. Response of the galvanometer when the step force is applied to the seismograph.

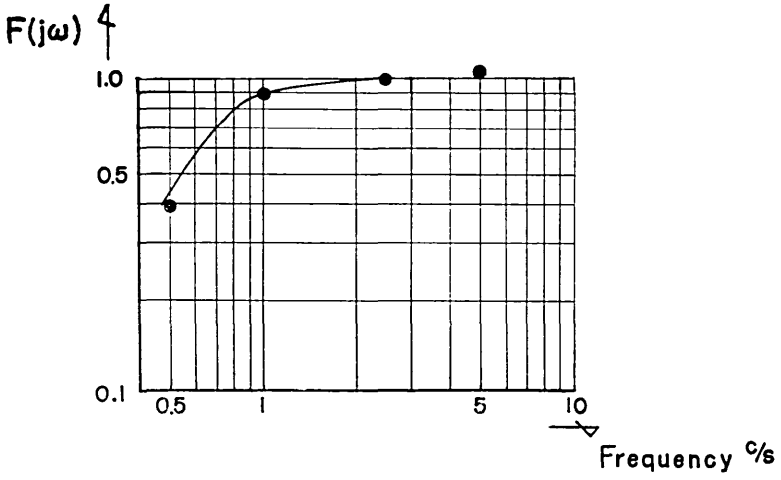

Fig. 12. $F(j\omega)$ (calculated)

6. Concluding remarks

In the present paper, the author has outlined the bore-hole seismometer specially designed for observations of earthquake motions on the surface as well as at the bottom of a bore-hole.

The bore-hole seismometer consists of pendulums of Willmore suspension which are damped heavily by silicon-oil and the output voltages are proportional to the ground accelerations. Coupling this seismometer directly to a GU-52-B type galvanometer, we attained the magnification of 80. The frequency characteristics of this seismograph are flat in the frequency range 1 to 20 cycles per second.

We are continuing to observe earthquakes at Okubo (premises of the Building Research Institute) and at Marunouchi (premises of Tokyo Station). The seismometers and galvanometers working at Okubo are a little different from the type outlined in this paper. The h of the seismometer is smaller than that of the seismometer at Marunouchi, and the current sensitivity of the galvanometer is higher than that of the galvanometer at Marunouchi. So the overall magnifications are three times as large as those of Marunouchi. Depths of the seismometer at Okubo are 0.6, 4.6, 8.7, 13.5, 30.0 and 70.5 m respectively. And at Marunouchi, installation depths are about 0.6 and 20.0 m respectively.

In conclusion, the author wishes to express his sincere gratitude to Professor Hirosi Kawasumi who offered him valuable advise and constant encouragement. His thanks are also due to Mr. M. Sibano and others who kindly helped the author in the laboratory as well as in the field. Part of the expense for the present study was defrayed from the Fund for Experimental Scientific Research from the Ministry of Education.

Part 2

Automatic Correlator

1. Introduction

It is well-known that the response of a constant parameter linear system for an arbitrary disturbance is to be obtained by the Fourier's double integral or a convolution integral, provided we know the frequency or impulse response functions of the system.

To know these vibration characteristics, experimental approaches have been made, but being too elaborate as they are, more feasible

approaches have been sought and found in an analysis of the responses of the structure to irregular natural disturbances such as microtremors due to artificial and other causes. Recent progress in the theory and techniques of communication have made it possible to solve the problem very easily. The most powerful weapons found in the communication theory are harmonic analysers and correlators. The correlators or the instruments for calculating correlation functions play very important roles in these fields and promise to be very useful in application to the vibration theory. In view of these facts we constructed a model of an automatic correlator and used it for analyses of vibrations of civil engineering structures and ground. In the following, a brief explanation of the theory, construction and application of the correlator will be given.

2. Theoretical background

It is well-known that the output $y(t)$ of a constant parameter linear system for the input $x(t)$ is given by

$$y(t)=\int_0^\infty h(\tau)x(t-\tau)d\tau\,, \tag{13}$$

or

$$y(t)=\frac{1}{2\pi}\int_{-\infty}^{\infty}H(\omega)d\omega\int_{-\infty}^{\infty}x(\tau)e^{j\omega(t-\tau)}d\tau\,, \tag{14}$$

where $h(t)$ and $H(\omega)$ are the impulse and frequency response functions respectively, and in themselves constitute a Fourier transform pair, that is

$$H(\omega)=\int_0^\infty h(\tau)e^{-j\omega\tau}d\tau\,, \tag{15}$$

and

$$h(t)=\frac{1}{2\pi}\int_{-\infty}^{\infty}H(\omega)e^{j\omega t}d\omega\,. \tag{16}$$

Now our present problem is to find the $h(t)$ and $H(\omega)$ of the structure, and the simplest approach to it is the experimental application of a impulse $x(t)=x_0\delta(t)$ ($\delta(t)$: δ-function) or a simple harmonic force $x(t)=x_0e^{j\omega t}$ to the input. But the response $y(t)$ to the most irregular stationary ergodic random process $x(t)$ can also yield very important information of the system if properly analysed, as will be shown below.

It has been proved that the power spectral density functions $W_{11}(\omega)$.

$W_{22}(\omega)$ and $W_{12}(\omega)$ of the input and output are related each other through the frequency response function $H(\omega)$ of the system by the following formulae.

$$W_{22}(\omega)=|H(\omega)|^2 W_{11}(\omega)\,, \tag{17}$$

and

$$W_{12}(\omega)=H(\omega)W_{11}(\omega)\,, \tag{18}$$

while the $W(\omega)$'s are the Fourier transforms

$$W_{ij}(\omega)=\int_{-\infty}^{\infty}\varphi_{ij}(\tau)e^{-j\omega\tau}d\tau\,, \tag{19}$$

of the auto- or cross-correlation functions

$$\varphi_{11}(\tau)=\frac{1}{2T}\int_{-T}^{T}x(t)x(t+\tau)dt\,, \tag{20}$$

$$\varphi_{22}(\tau)=\frac{1}{2T}\int_{-T}^{T}y(t)y(t+\tau)dt\,, \tag{21}$$

and

$$\varphi_{12}(\tau)=\frac{1}{2T}\int_{-T}^{T}x(t)y(t+\tau)dt\,, \tag{22}$$

respectively. We can therefore know the frequency response function of the system $H(\omega)$ by the Equations (17) and (18) from the correlation functions (20), (21) and (22) through the Fourier transformation (19).

As the inverse Fourier transform of (19) is

$$\varphi_{ij}(\tau)=\frac{1}{2\pi}\int_{-\infty}^{\infty}W_{ij}(\omega)e^{j\omega\tau}d\omega\,, \tag{23}$$

we have

$$\varphi_{12}(\tau)=\frac{1}{2\pi}\int_{-\infty}^{\infty}H(\omega)W_{11}(\omega)e^{j\omega\tau}d\omega\,, \tag{24}$$

and

$$\varphi_{22}(\tau)=\frac{1}{2\pi}\int_{-\infty}^{\infty}|H(\omega)|^2 W_{11}(\omega)e^{j\omega\tau}d\omega\,, \tag{25}$$

from which we can easily deduce the following formulae, when the input is white noise, that is $W_{11}(\omega)=const=C$.

$$\varphi_{12}(\tau)=\frac{C}{2\pi}\int_{-\infty}^{\infty}H(\omega)e^{j\omega\tau}d\omega=Ch(\tau)\,, \tag{26}$$

and

$$\varphi_{22}(\tau)=\frac{C}{2\pi}\int_{-\infty}^{\infty}H(\omega)H^{*}(\omega)e^{j\omega\tau}d\omega=C\int_{-\infty}^{\infty}h(t)h(t+\tau)dt$$
$$=C\varphi_{hh}(\tau)\,. \tag{27}$$

In the above equation, $H^{*}(\omega)$ denotes the conjugate complex of $H(\omega)$. It can be shown when

$$h(t)=Ae^{-\varepsilon t}\sin\sqrt{n^2-\varepsilon^2}\,t \qquad 0\leqq t\,,$$
$$=0 \qquad 0>t\,, \tag{28}$$

that

$$\varphi_{hh}(\tau)=\frac{A^2}{4n^2\varepsilon}e^{-\varepsilon\tau}\cos\left(\sqrt{n^2-\varepsilon^2}\,\tau-\theta\right),$$
$$\tan\theta=\varepsilon/\gamma\,. \tag{29}$$

It will be worth noting that the auto-correlation function of the output or the cross-correlation function of the input and output of the linear system responding to the input white noise is by itself the free oscillation of the system, so that we can easily determine the proper period and the damping of the linear system from $\varphi_{22}(\tau)$ or $\varphi_{12}(\tau)$.

3. Principle of construction

To calculate the correlation functions defined by the Equations (20), (21) and (22), it is necessary to use repeatedly values of say $f(t)$ and $g(t)$ at different times. It is therefore convenient to have these values memorized, so that they may be easily recalled.

To comply with the requirements we used electric signals of the analogue type for $f(t)$ and $g(t)$, and adopted the magnetic recording method for the electric signals. Considering the high fidelity in the amplification and recording as well as the feasibility in the calculation of the products and integrals involved in the correlation functions, the electric signals $f(t)$ and $g(t)$ are pulse-width modulated although in the calculation stage one of them is demodulated back to the original analogue form as will be stated below.

Since four values $f(t)$, $g(t)$, $f(t+\tau)$ and $g(t+\tau)$ are involved in the calculations for $0\leqq\tau$, and magnetic heads for recording and reproducing are finite in their magnitude, these four values are to be recorded simultaneously on separate tracks on a single tape. We therefore used a tape $\frac{1}{2}$ inch wide, and placed two heads of $f(t)$ and $g(t)$ parallel at a

position, and the others for $f(t+\tau)$ and $g(t+\tau)$ also parallel at a different position.

By changing a little the length of the tape lying between these pairs of heads in the reproducing process, we can obtain $f(t)$ or $g(t)$ and $f(t+\tau)$ or $g(t+\tau)$ of variable τ simultaneously, and the requirement for τ to be $0 \leqq \tau$ is thus secured.

The multiplication of say $f(t)$ and $g(t+\tau)$ is carried out by chopping the demodulated signal $g(t+\tau)$ by the pulse width modulated signal of $f(t)$, so that we have a trapezoidal pulse, repeating according to the sampling rate of the pulse width modulation. As the height and width of this pulse is proportional to $g(t+\tau)$ and $f(t)$ respectively, the electric charge transported by this impulse is proportional to the product $f(t)\cdot g(t+\tau)$. We can therefore obtain a point of the correlation function $\varphi_{12}(\tau)$ by integrating the charge of these product. This integration is made by means of a condenser.

Our analyser is based on the above principle, and is so made as to perform these calculations automatically, and record the integral, say

$$\int_0^t f(t)g(t+\tau)dt=\varphi(t,\tau)\,,$$

automatically up to $t=T-\tau$, and to stop at the end and to return to the initial zero position. It then renews its function after increasing the value of τ by a prescribed amount. All these processes are repeated automatically so that we are able to gain the desired correlation function by drawing an envelope of the recorded $\varphi(t,\tau)$ curves.

4. Actual construction

A photograph of our apparatus is shown in Photo. 1, and its block diagram in Fig. 13.

It consists of four units, a) memory unit, b) delay time controller, c) reproducing and calculating unit and d) recorder.

Specifications are as follows:

1) Input signal : 0.5 V (p-p), 0–20 cps.
2) Input resistance : 5 K Ω
3) Demodulated output : 1 V (p-p), 0–100 cps.
4) Output resistance : 5 K Ω
5) Magnetic tape : $\frac{1}{2}$ inch wide, 3 m long endlessly pasted.
6) Tape speed : 8 cm/sec for recording, 40 cm/sec in reproducing.
7) Power consumption : about 100 watts.

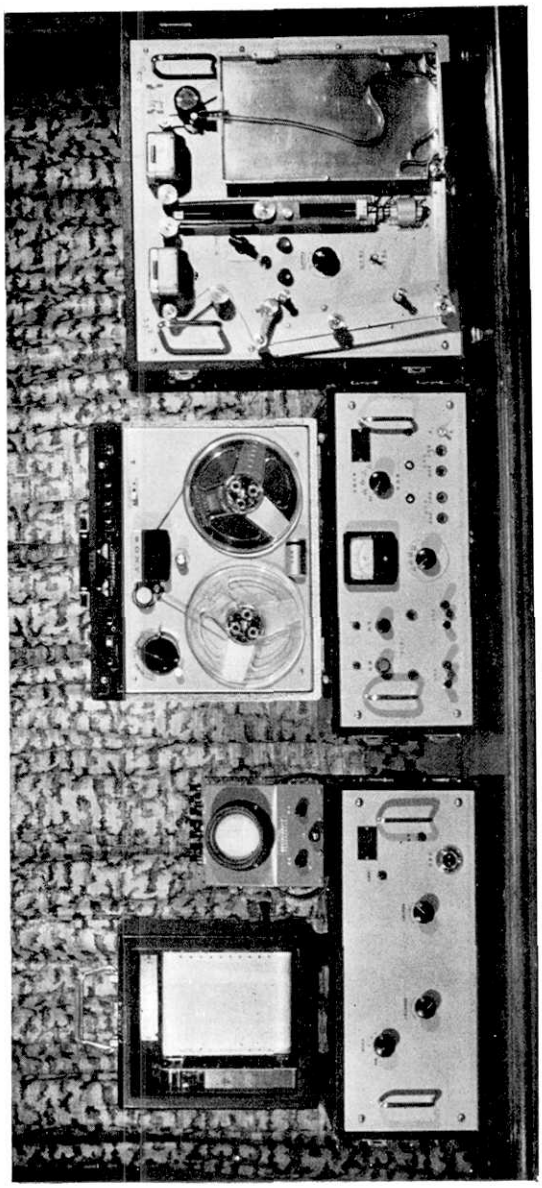

Photo. 1.

Now let us explain in a little more detail each of the respective units of our apparatus.

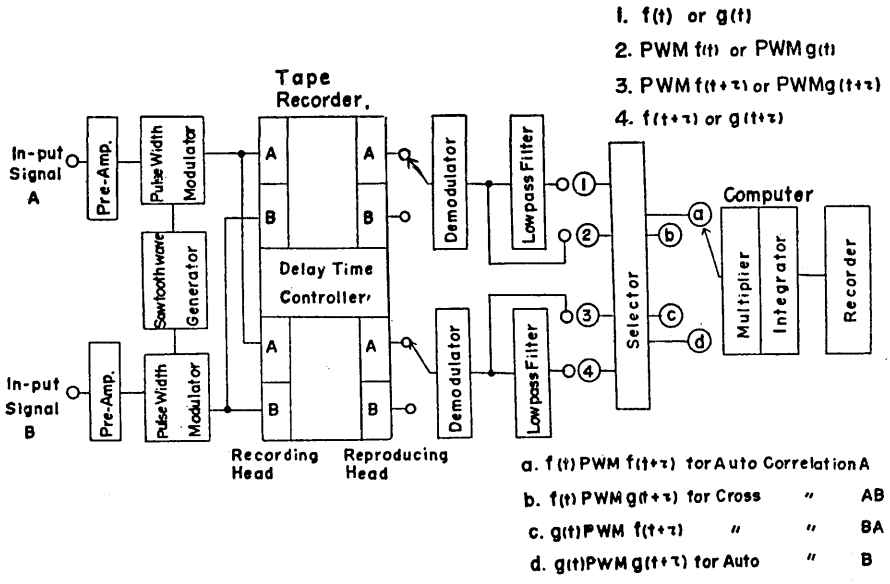

Fig. 13. Block diagram of the automatic correlator.

a) Memory unit

The input signals are amplified by the transistorized DC preamplifier and are modulated by the pulse width modulation system. The pulse width modulated signals are derived easily by changing the slicing level of the saw-tooth waves in proportion to the input signal. The saw-tooth wave generator is contained in this unit, and the repetition frequency of the waves (which we call "sampling rate") is 120 times per second. The modulated signals are amplified once more and fed directly to the magnetic tape recorder. To comply with the above requirements, two pairs of the same signals of $f(t)$ and $g(t)$ are recorded on the tape at different positions as shown in Fig. 13. So, four tracks are recorded on the tape simultaneously.

b) Delay time control machanism

The delay time "τ" between the two time functions, is obtained by changing the length of the tape lying between the fixed heads. This operation is accomplished as stated below (see Fig. 14).

i) A piece of tin-foil, 1 cm wide and 3.5 cm long, which is stuck on

the endless tape, passes by the contactor 1, and makes a circuit, by which,

ii) a contact signal is sent to the relay, to halt the movement of the magnetic tape.

iii) At the same time, a motor for shifting down the movable guide roller a prescribed amount is brought into play for a moment. By this operation, the length of the tape between the two fixed heads is increased.

iv) After completing this action, the circuit for driving the tape is made.

v) Then the tin-foil contacts contactor 2, and the next calculation is started.

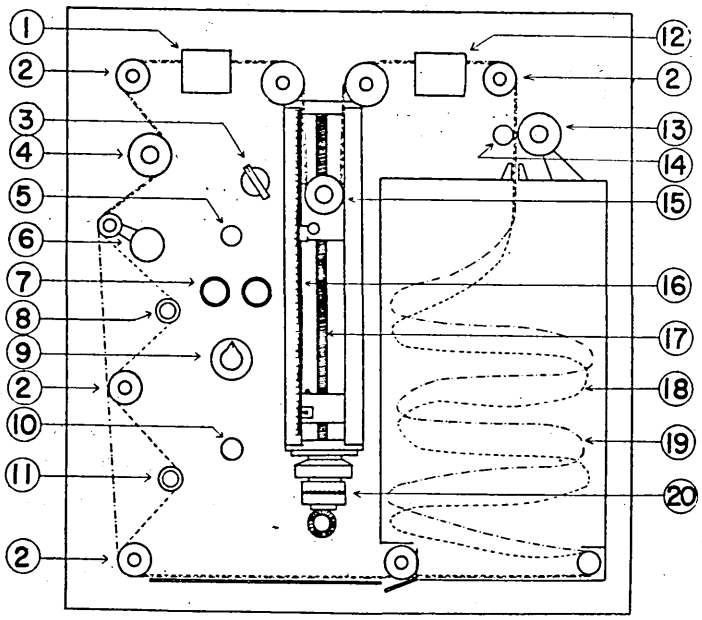

Fig. 14. Schematic view of the memory unit. (1) Recording head A, (2) guide roller, (3) tape speed selector, (4) flywheel, (5) pilot lamp, (6) tension arm, (7) push buttons, (8) contactor 2, (9) delay time selector, (10) transfer switch, (11) contactor 1, (12) recording head B, (13) pinch roller, (14) capstan, (15) delay time controlling guide roller, (16) delay time scale, (17) feed screw, (18) tape (reproducing stage), (19) tape (recording stage), (20) adjuster.

Thus, the whole cycle of calculating $\varphi(\tau)$ is repeated automatically. And at last the movable guide roller slides down the whole length of the delay time scale, when a contact maker breaks the power circuit, and

the whole function of the correlator is stopped.

In our apparatus, available delay time increments at one time are 1/40 sec., 1/80 sec. and 1/160 sec. respectively. We may select one of these increments which will be suitable for the frequency characteristics of the input signals. And, if necessary, we may also select arbitrary delay times by a manual shifting of the guide roller.

c) *Reproducing and calculating unit*

In the calculation process, we first reproduce two of the four recorded signals from the tape, depending on the problem. For instance, if we want to calculate an auto-correlation function, we reproduce $f(t)$ and $f(t+\tau)$ or $g(t)$ and $g(t+\tau)$. In the case of a cross-correlation function we reproduce $f(t)$ and $g(t+\tau)$ or $f(t+\tau)$ and $g(t)$. Because of the differential characteristics of the reproducing heads, the pulse position modulated signals are derived from the tape as outputs. And we change them again to the pulse width modulated signals for convenience' sake in the latter calculations.

Now the multiplication of the two functions is explained. This is done as follows: (As an example, we will explain the case of the cross-correlation function of $f(t)$ and $g(t)$.)

i) One of the signals, say $g(t+\tau)$, is demodulated by the low pass filter.

ii) And chopping this by the other pulse width modulated signal, we obtain a series of trapezoidal pulses whose height and width are proportional to $g(t+\tau)$ and $f(t)$ respectively.

iii) We sent these waves through the low pass filter.

By the output current of the filter, we charge the condenser during one cycle of the calculation.

Now the voltage across the condenser is proportional to a value of the correlation function between $f(t)$ and $g(t+\tau)$ for a given τ. This voltage is amplified and the result is fed to the recorder.

In our apparatus, a KR-type penwriter of YEW is used as a recorder. At every end of the calculation cycles the tape is stopped and to prepare for the next cycle, a condenser is clamped by a constant voltage and the pen swings back quickly to the zero position. The necessary time of one calculation cycle is about 7.5 seconds. In this way the calculations are repeated over and over again until the delay time "τ" between the two functions becomes sufficiently large. The results of these calculations are recorded at constant intervals on a sheet of paper driven very slowly, so that the correlation function is easily given as

the envelope of these curves.

Theoretically, the value of the auto-correlation function should be maximum at the zero delay time. But from the practical point of view, as we use a low pass filter, the lag of the physically realizable low pass filter should be considered. In our apparatus this time lag is about 6.5 milli-seconds. And we may say that this value is constant in the frequency range of interest.

At the end of this article, it should be noted that, because the circuits of this apparatus are all transistorized, the whole equipment is made smaller and lighter than any other which has hitherto been made.

5. Calculated examples

In Figs. 15 and 16, the examples worked out are given. Figs. 15a and 15b are examples of auto-correlation functions, where the input

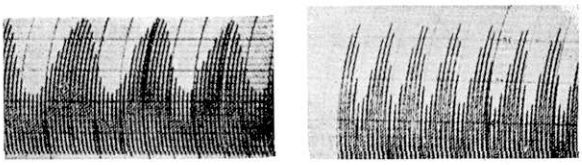

a b

Fig. 15. Examples of calculated auto-correlation functions of sine wave of (a) 2cps, ($\Delta\tau=0.027$ sec.), (b) 20cps, ($\Delta\tau=0.0068$ sec.)

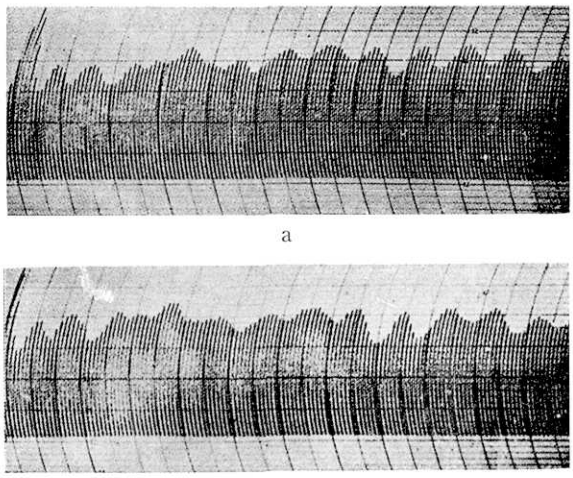

a

b

Fig. 16. Auto-correlations of the natural minute irregular motions (so-called microtremors) observed at the second floor of the Earthquake Research Institute as calculated at different times from the same record. ($\Delta\tau=0.027$ sec.)

signals are derived from a very low wave generator (oscillator). These examples will show that the correlator works satisfactolily. To test the stability of the function of our correlator, we calculated at different times from the same record the auto-correlation functions of the microtremors observed from the 2nd floor of the Earthquake Research Institute. The results which are shown in Figs. 16a and 16b are exactly the same, and this shows that the correlator works very stably. Figs. 17a through 17d are examples showing the validity of the above-mentioned equations, in that we can obtain free vibrations of structures by our apparatus from microtremor observations.

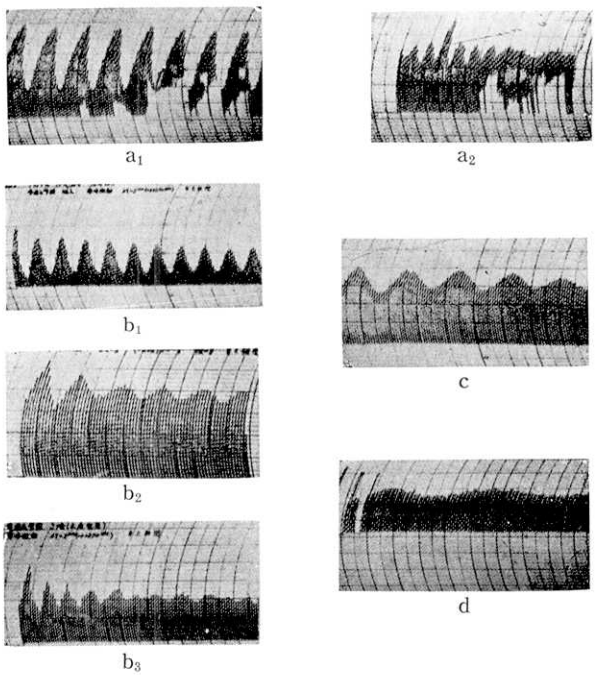

Fig. 17. Auto-correlations of the natural minute irregular motions of structures. The observations were made (a_1), (a_2) at the top of an arch-dam; (b_1) on the ground, (b_2) on the second floor of a wooden building, (b_3) on the ground floor of a RC building on the margin of up-town Tokyo; (c) on the roof of a 7-storied framed building; (d) at the 130 m level of a TV tower. (a): $\Delta\tau = 0.011$ sec., (b), (c), (d): $\Delta\tau = 0.027$ sec.

6. Acknowledgements

The author expresses his hearty thanks to Professor Hirosi Kawasumi who gave him valuable advice and encouragement. The author's

thanks are also due to the staff of Sony Corporation who gave him technical assistance and many facilities. The author wishes to acknowledge the assistance of the Ministries of Education and of Construction in providing funds to enable the apparatus to be constructed. Without their collaboration and aid this correlator would not have been brought into being.

Part 3

Frequency Characteristics of the Superficial Soil Layers

1. Introduction

Observation in the depths of the ground is indispensable if we are to clarify the frequency characteristics and behavior of the stratified media. These observations at the same time make it possible to check the thory of the reflection and the refraction of the seismic waves near the surface. T. Matuzawa[37] once pointed out the necessity of underground observation. And lately the importance of this kind of study has been largely recognized even in the engineering fields in order to gain the necessary information for earthquake proof constructions.

However, a lack of suitable seismographs for this purpose has impeded progress so that until now very little research on the present problem has been published. It was indeed a very troublesome and tremendous task to set a seismograph of direct mechanical or optical recording in the depths of the ground and to maintain its stable operation. For example, Saita and Suzuki[38] were obliged to use a big well to set an accelerometer and to bear all the hardships of going down to the bottom to obtain the seismograms. Moreover, under these circumstances, nearby soil conditions had to be altered. Recently, K. Kanai and others[39] have began comparative observations of earthquakes in the gallery of the Hitachi Mine and at the surface. The same type of study was carried out by Nakamura[40] and Nasu[41] near Atami and at Tanna respectively. But influences from the surrounding conditions would have to be taken into consideration in the case of these studies.

37) T. MATUZAWA, *Zisin*, **4** (1932), 125.
38) *loc. cit.*, 15).
39) *loc. cit.*, 20).
40) *loc. cit.*, 11).
41) *loc. cit.*, 12).

In avoiding the effect of surrounding influences, it may be claimed that our efforts were successful, because our bore-hole seismometer could be set at the bottom of a small bore-hole and buried again. This observation of underground earthquake motions in such a natural condition was perhaps the first one ever made.

We are continuing observations of earthquakes at both Okubo and Marunouchi. Part of the study of the seismograms recorded at Marunouchi is hereby reported.

2. Comparative observations of earthquakes under the ground and on the surface

In April of 1960, comparative observations of earthquakes under the ground and on the surface were started at two places about 200 m apart on the premises of Tokyo Station on the Marunouchi side. The depths of the bore-holes at each place are 20.5 and 21.2 m respectively. The location of each bore-hole is given in Fig. 18. Surface seismometers were buried near each bore-hole at depths of 0.9 and 0.8 m respectively. The symbols used and the sensitivity of each seismograph are listed in Table 6.

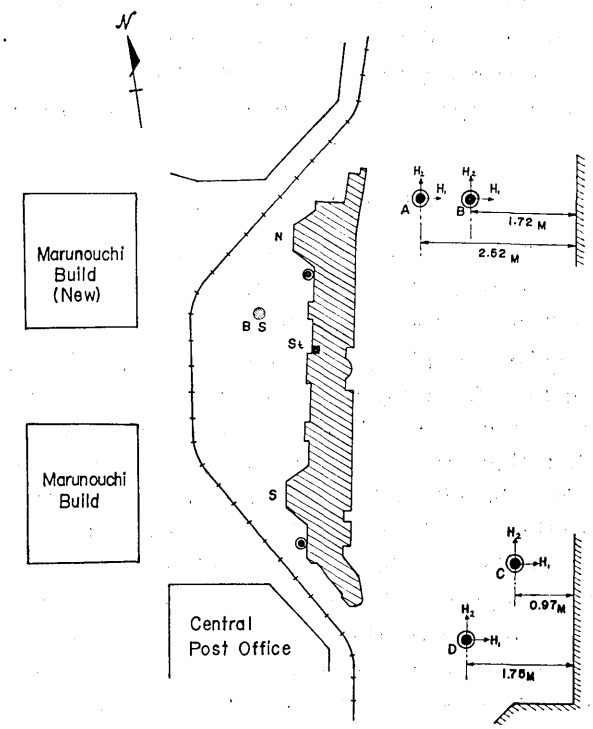

Fig. 18. Location of each bore-hole and temporary station.

The galvanometers were installed in the attic of the station building. The paper speed of the record was selected to be 1 cm/sec in order to gain clear legible seismograms, and the time marks of 1 sec-intervals are recorded in the seismograms. For routine observation, we used a starter. This device starts the function of recording ap-

paratus with the initial motions of the earthquake and stops the function after 1 minute, and awaits the next shock.

Table 6.

Location		Symbol used	Component	Depth from the surface in m	Magnification
Near the North Entrance of Tokyo Station of Marunouchi side	Surface	$N\text{-}BH_1$	EW	0.9	80
	Bottom	$N\text{-}AH_1$	EW	20.5	80
Near the South Entrance of Tokyo Station of Marunouchi side	Surface	$S\text{-}CH_1$	EW	0.8	65
	Bottom	$S\text{-}DH_1$	EW	21.2	65

We can record three seismograms on a single recording paper. Sometimes we fail to record the seismograms, because the recorder is forced to move many times by artificial disturbances and there is no space left on the paper for recording a new earthquake.

3. Geological aspects of the environment of Marunouchi[42]

The damage to wooden dwelling houses caused by earthquakes is known to be heavier in the down-town area than in the up-town district of Tokyo. From the view point of earthquake engineering, this fact is ascribed mainly to the physical properties of the superficial formations. Surface formations in the up-town area are diluvia, and those in the down-town are alluvia. The diluvial deposits are compacted so closely that they are generally used as a supporting bed for large buildings, while the alluvial formations are very soft and are not capable of supporting building foundations. So, information relating to the physical properties of the deposits and information on the geological as well as the geographical conditions is indispensable for our study.

Now, from the geographical point of view, the up- and down-town margin is a clearly marked line connecting Ueno, the Imperial Palace and Shinagawa. Marunouchi is located near the western boundary of the down-town area and its geological aspects are summarized in Table

42) Dr. K. Suyama of Fukada Geological Institute kindly acquainted the author with details of the geology of the Marunouchi area. The author's sincere thanks are due to him.

7. In Fig. 19[43], we show a profile of the geological formations near Tokyo Station.

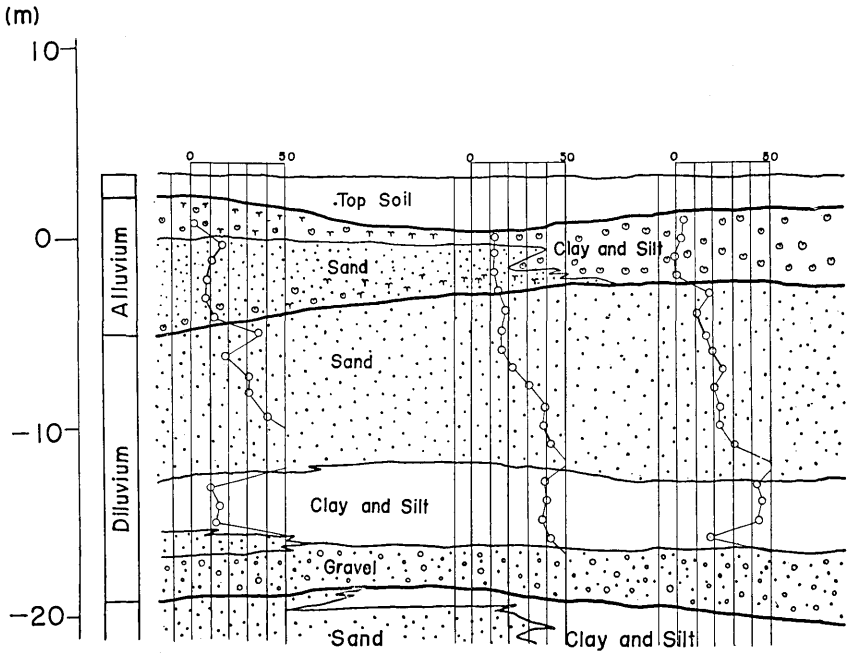

Fig. 19. Geological formations near Tokyo Station, and the number of blows N in standard penetration test.

As we see in Fig. 19, the depth of the bore-hole for our seismometer agrees with that of the top of the Tokyo gravel-bed. The thicknesses of the alluvial and diluvial formations above the Tokyo gravel-bed are approximately 6 m and 14 m respectively.

4. The results of the observations

22 earthquakes were observed on the premises of Tokyo Station on the Marunouchi side, from April to September of 1960. The main earthquakes observed are listed in Table 8. The epicenters of these earthquakes are shown in Fig. 20.

During this period, observations were made only of the EW-component[44]. The seismograms are shown in Fig. 21 through Fig. 28.

43) Courtesy of the Fukada Geological Institute.

44) From October of 1960, we started to record the NS-component, too. So, we are able to record 8 simultaneous seismograms of each earthquake.

Table 7.

Geology of Tokyo Station and its neighbourhood

Age	Division	Lithologic Facies	Number of blows (N) (Standard Penetration Test)	
			Cohesive Soil	Sand
	Top Soil and Fill	Mainly clay and clay-silt, with artificial fills	5±	
Holocene*	Yurakucho Formation	Mainly clay and silt "Generally the Yurakucho Formation is divided into three parts. The upper Yurakucho Formation (mainly sand), the middle Yurakucho Formation (soft clay), the lower Yurakucho Formation (mainly sand and gravel)"	3±	20±
	~ (unconformity) ~			
Pleistocene**	Tokyo Formation	Upper part (thickness less than 15 m) Mainly sand, intercalating clay	10±	40±
		Middle part (thickness 3~6 m) Sand and gravel		50±
		Lower part (thickness more than 15 m) Mainly sand	50±	50±

* (Alluvium)
** (Diluvium)

Table 8.

Rec. No.	Epicenter Latitude	Epicenter Longitude	Epic. Dist. km	Time of occurence Month	Date	h	m	Reference
								Depth
R— 9	35.5 N.	140.2 E	43	6	9	13	21	h=70 km
R—10	35.7	140.4	56	6	26	9	00	h=80 km
R—12	35.4	140.4	64	7	18	14	40	h=40 km
R—15	40.3	142.4	565	7	30	02	32	h=40 km
R—16	36.4	141.5	171	8	12	22	12	h=40 km a. c. M=5.9
R—19	35.1	140.2	73.5	8	25	17	38	h=60~70 km
R—20	36.4	140.7	102.5	8	26	18	20	h=60 km a. c. M=5
R—21	35.9	140.5	70.5	9	01	07	51	h=40 km

Now, glancing at these records, the following features can be clearly observed.

i) Seismograms recorded underground are much simpler than those recorded on the surface.

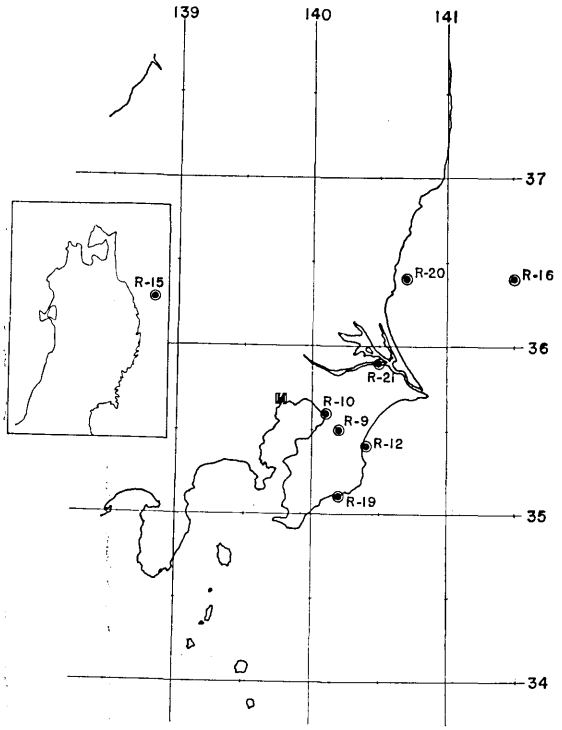

Fig. 20. Epicenters of main earthquakes observed on the premises of Tokyo Station.

ii) Amplitudes of the surface are always bigger than those of the underground.

iii) With respect to the long-period waves, close similarities are found between the two seismograms.

iv) The records have the tendency to show that the larger the epicentral distance, the better similarities are observed.

v) Predominant waves with a large amplitude and definite period which may be considered as the proper period of the subsoil are found in the seimograms.

With regard to these points, former investigators compared only the maximum amplitudes of seismograms or their period-frequency curves. We shall, however, take a different approach by calculating Fourier transforms of each seismogram to compare them. Thus more precise characteristics of the strata will be noted than ever before.

5. Theoretical background of the frequency analysis of the seismograms

If the seismogram $f(t)$ consists of repetitive waveforms, we may express it by the Fourier series. This is valid, only if the following condition exists.

$$\lim_{T\to\infty}\frac{1}{T}\int_{-\frac{T}{2}}^{\frac{T}{2}}\{f(t)\}^2dt<\infty\ , \tag{30}$$

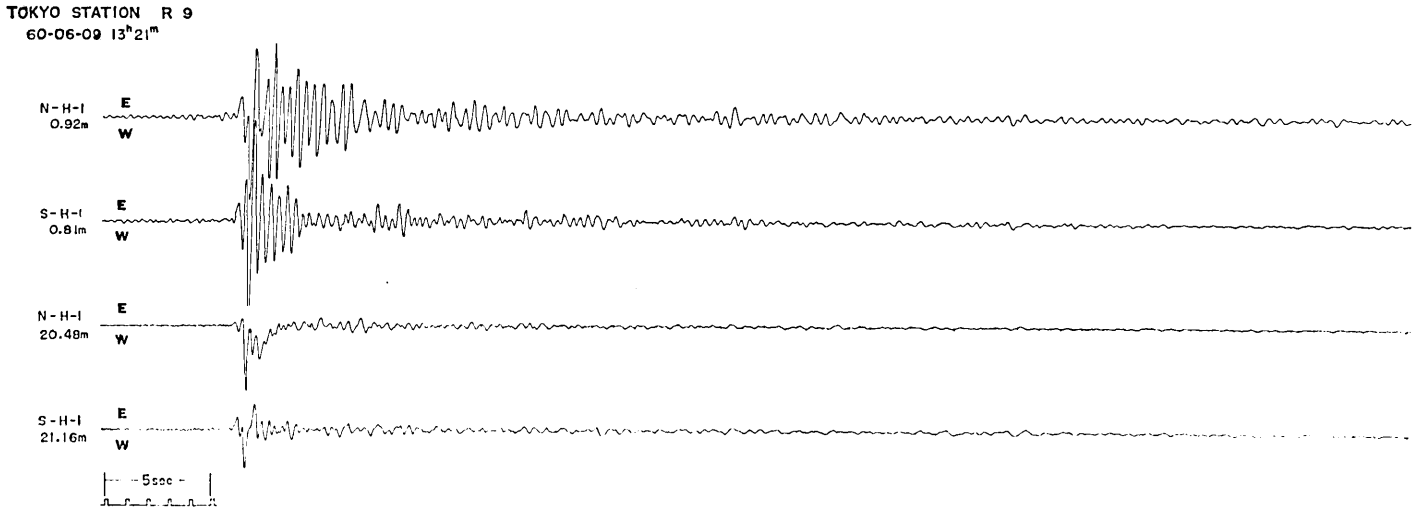
TOKYO STATION R 9
60-06-09 13h21m
N-H-1 0.92m E W
S-H-1 0.81m E W
N-H-1 20.48m E W
S-H-1 21.16m E W
5sec

Fig. 21.

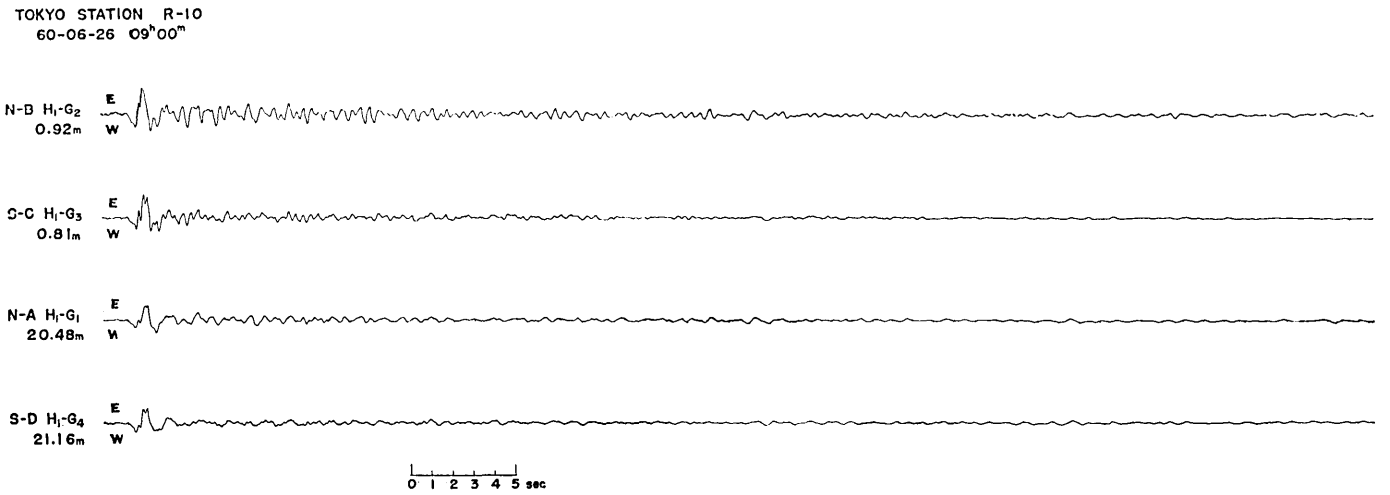
TOKYO STATION R-10
60-06-26 09h00m
N-B H1-G2 0.92m E W
S-C H1-G3 0.81m E W
N-A H1-G1 20.48m E W
S-D H1-G4 21.16m E W
0 1 2 3 4 5 sec

Fig. 22.

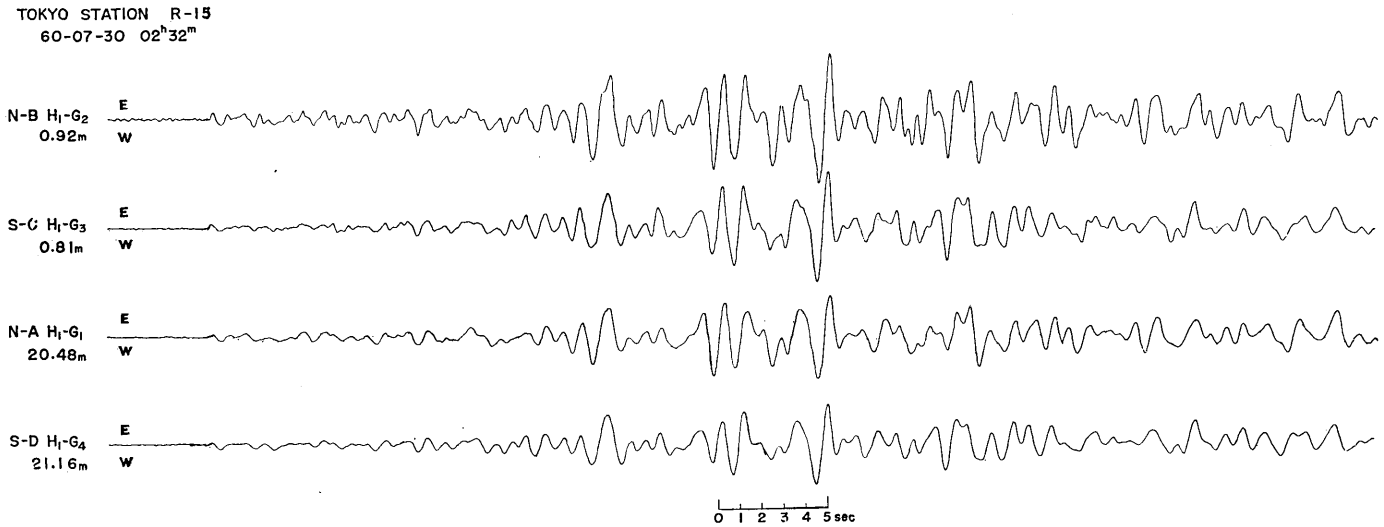
TOKYO STATION R-15
60-07-30 02h32m
N-B H1-G2
0.92m
E
W
S-C H1-G3
0.81m
E
W
N-A H1-G1
20.48m
E
W
S-D H1-G4
21.16m
E
W
0 1 2 3 4 5 sec

Fig. 23.

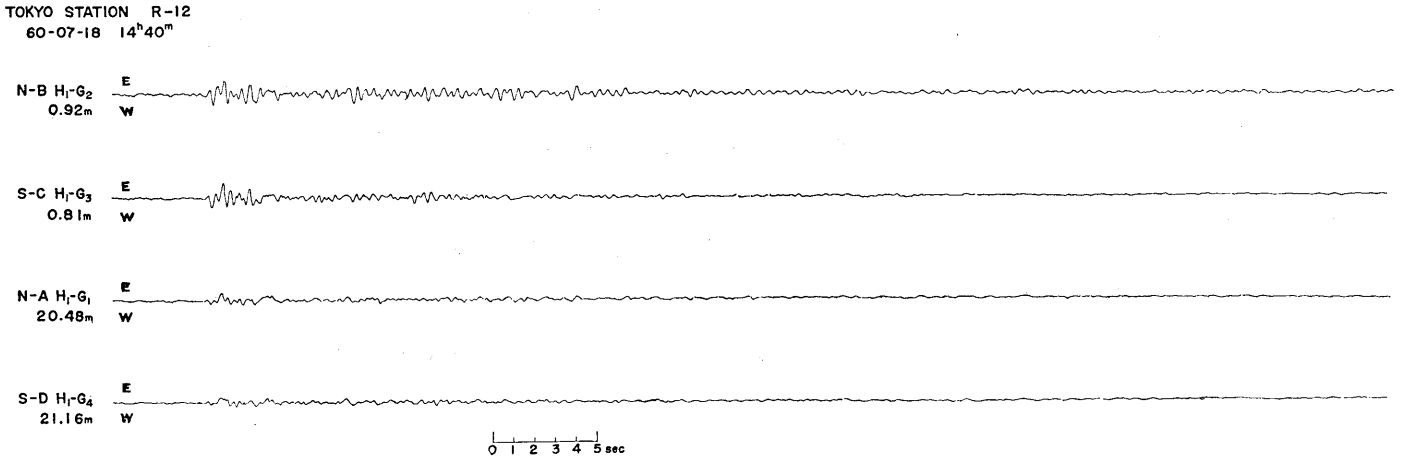
TOKYO STATION R-12
60-07-18 14h40m
N-B H1-G2
0.92m
E
W
S-C H1-G3
0.81m
E
W
N-A H1-G1
20.48m
E
W
S-D H1-G4
21.16m
E
W
0 1 2 3 4 5 sec

Fig. 24.

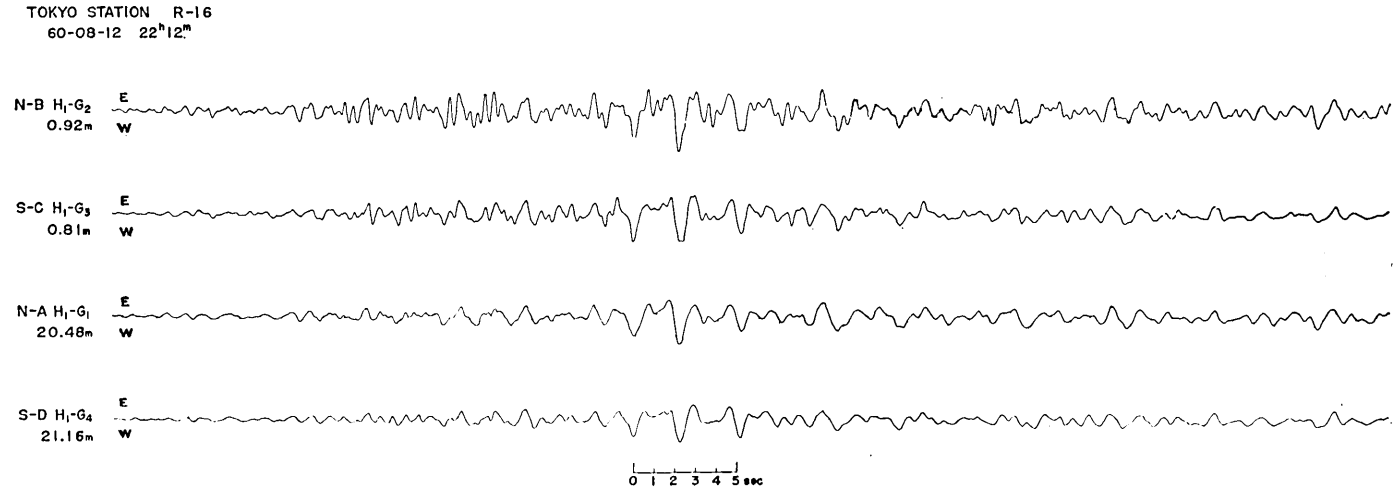
TOKYO STATION R-16
60-08-12 22h12m
N-B H1-G2
0.92m
S-C H1-G3
0.81m
N-A H1-G1
20.48m
S-D H1-G4
21.16m
E
W
0 1 2 3 4 5 sec

Fig. 25.

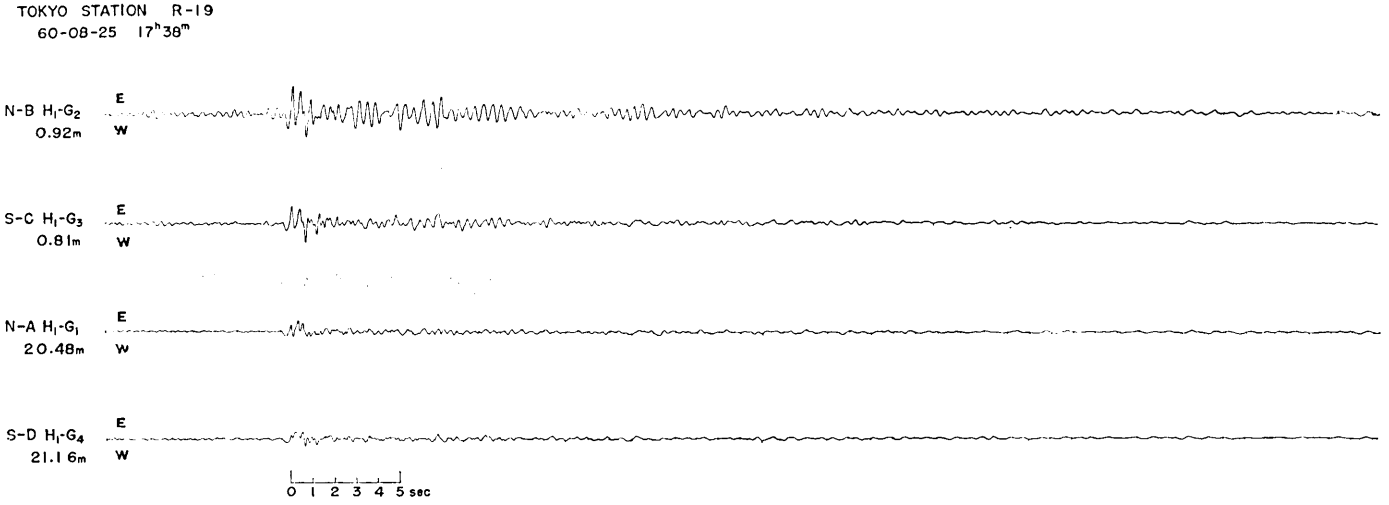
TOKYO STATION R-19
60-08-25 17h38m
N-B H1-G2
0.92m
S-C H1-G3
0.81m
N-A H1-G1
20.48m
S-D H1-G4
21.16m
E
W
0 1 2 3 4 5 sec

Fig. 26.

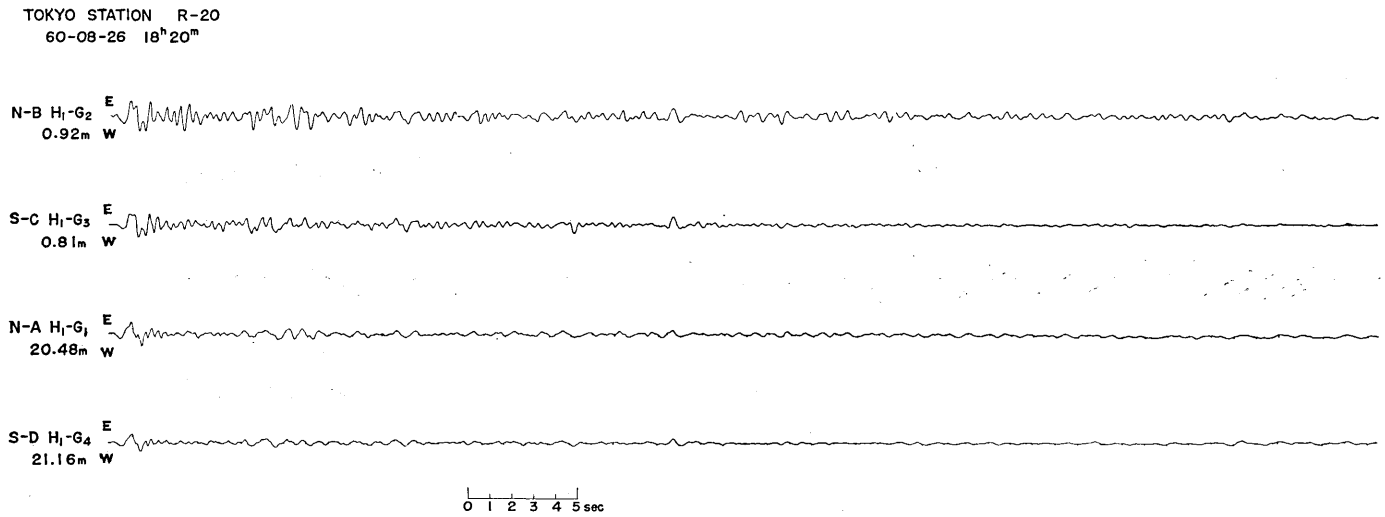
TOKYO STATION R-20
60-08-26 18h20m
N-B H1-G2 E
0.92m W
S-C H1-G3 E
0.81m W
N-A H1-G1 E
20.48m W
S-D H1-G4 E
21.16m W
0 1 2 3 4 5 sec

Fig. 27.

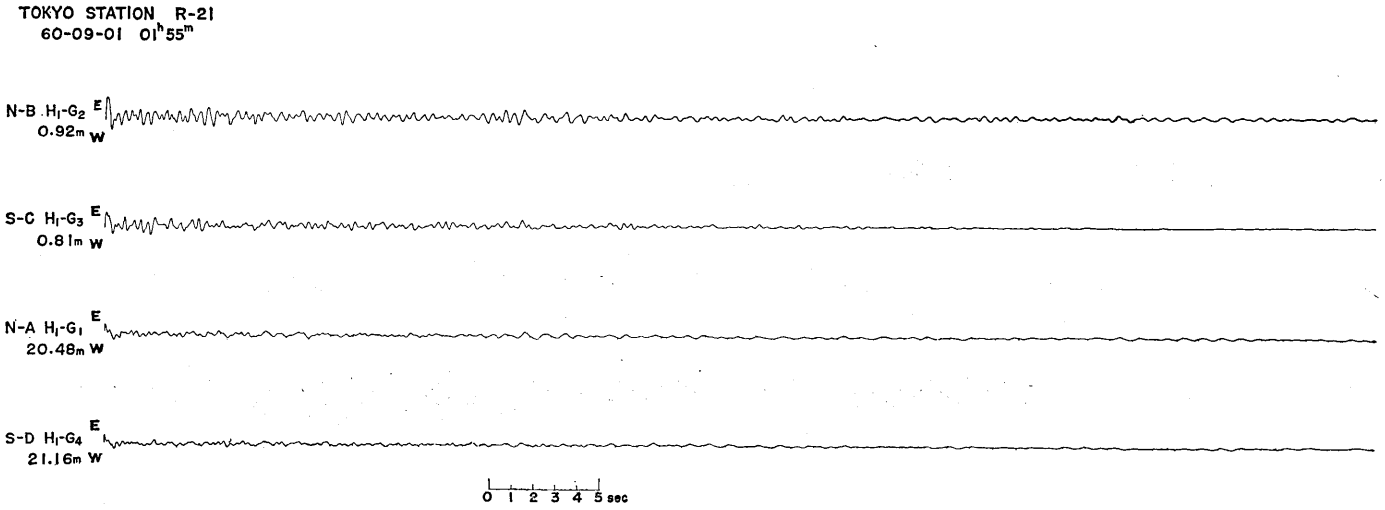
TOKYO STATION R-21
60-09-01 01h55m
N-B H1-G2 E
0.92m W
S-C H1-G3 E
0.81m W
N-A H1-G1 E
20.48m W
S-D H1-G4 E
21.16m W
0 1 2 3 4 5 sec

Fig. 28.

where T is the period of repetition. We may say that the power of $f(t)$ is finite in such a case. In other words, $f(t)$, which can be expressed by the Fourier series, must be a periodic function which lasts for ever. Accordingly, the energy of such a wave becomes infinity. Notwithstanding the severe restriction, Fourier analyses have been used with great popularity in our field to analyse the waveforms. However, in many branches of geophysics, particularly in seismology, we have to analyse transient phenomena such as the earthquake motions. These waveforms, which are finite in duration, satisfy the condition

$$\int_{-\infty}^{\infty} \{f(t)\}^2 dt < \infty \,. \tag{31}$$

The energy of the wave is finite in this case. Fourier expansion is no longer applicable to such a case, but the theory of the Fourier integral can be used conveniently to analyse such a waveform.

Let us now denote the waveform of the earthquake as $f(t)$, and assume that $f(t)$ is zero everywhere outside the range from t_1 to t_2. Namely,

$$f(t) \equiv 0 \qquad \text{for} \qquad |t-t_0| > \frac{T}{2} \,, \tag{32}$$

where $t_1+t_2=2t_0$, and $t_1-t_2=T$.

Expanding $f(t)$ in the Fourier series, in the range from t_1 to t_2, we have

$$f(t)=r(t)\sum_{n=-\infty}^{\infty} c_n e^{jn\omega_0 t} \,, \tag{33}$$

where $\omega_0=2\pi/T$, and,

$$\begin{aligned} r(t)&=1 \qquad |t-t_0|<\frac{T}{2} \,, \\ &=0 \qquad >\frac{T}{2} \,, \end{aligned} \tag{34}$$

$$c_n=\int_{t_0-\frac{T}{2}}^{t_0+\frac{T}{2}} f(t)e^{-jn\omega_0 t}dt \,. \tag{35}$$

Now the frequency representation of $f(t)$ is derived as,

$$\Omega(\omega)=\int_{-\infty}^{\infty} f(t)e^{-j\omega t}dt \,. \tag{36}$$

From Equations (33) through (36), we have,

$$c_n=\frac{1}{T}\Omega(n\omega_0)\,. \tag{37}$$

Equation (37) is a very important formula, which shows the relationships between the Fourier's coefficients and the sampling values of the Fourier transformation. Now, using the sampling theorem in the time domain, that is "if a function $f(t)$ contains no frequencies higher than f cycles per second, it is completely determined by giving its ordinates at a series of points spaced $\frac{1}{2}f$ seconds apart, the series extending throughout the time domain,"[45] we read off the $2Tf$ values from the seimogram at equal intervals, and expand them in the Fourier series everywhere in the range from t_1 to t_2. After the above calculation, multiply the Fourier coefficient by (t_2-t_1), and we have the approximate Fourier transform (continuous spectrum) connecting each line spectrum by a smooth curve. And values thus obtained satisfy the necessary condition of the frequency domain. If we want an accurate one, we can calculate it from an analytical expression of $\Omega(\omega)$, in terms of its values at the sampling points.

$$\Omega(\omega)=\sum_{n=-\infty}^{\infty}\Omega\left(\frac{2\pi n}{T}\right)\frac{\sin\left(\frac{\omega}{2}T-\pi n\right)}{\left(\frac{\omega}{2}T-\pi n\right)}\,. \tag{38}$$

6. Results of analyses

Seismograms of five earthquakes, R-9, R-10, R-12, R-19 and R-20 respectively, were analysed at this time. Consequently, we have analysed twenty seismograms. As we see in Table 9, the epicentral distances of these earthquakes were below 100 km. As for earthquakes of large epicentral distances, the analyses are under way, and the results will be reported at the earliest opportunity.

For the actual analyses, we enlarged every 11 seconds the principal portion of the seismograms 6.5 times of the original, and read off 720 sampling points on each seismogram. The analysed parts of the seismograms are believed to be the motion due to shear-waves. Considering the frequency characteristics of the seismograph, we omitted the period above 2 seconds from our discussion, because, as we see in Fig. 12 of

45) S. GOLDMAN, *Information Theory*, Prentice-Hall. Inc., 1953.

Part 1, the magnification of the seismograph decreases acutely at that frequency.

The results of analyses are shown in Fig. 29 through Fig. 38. Glancing over the results, we could find that there are two cases. One is the case where the spectral intensities of the surface and the underground motions change in the same phase. The other is the case where the

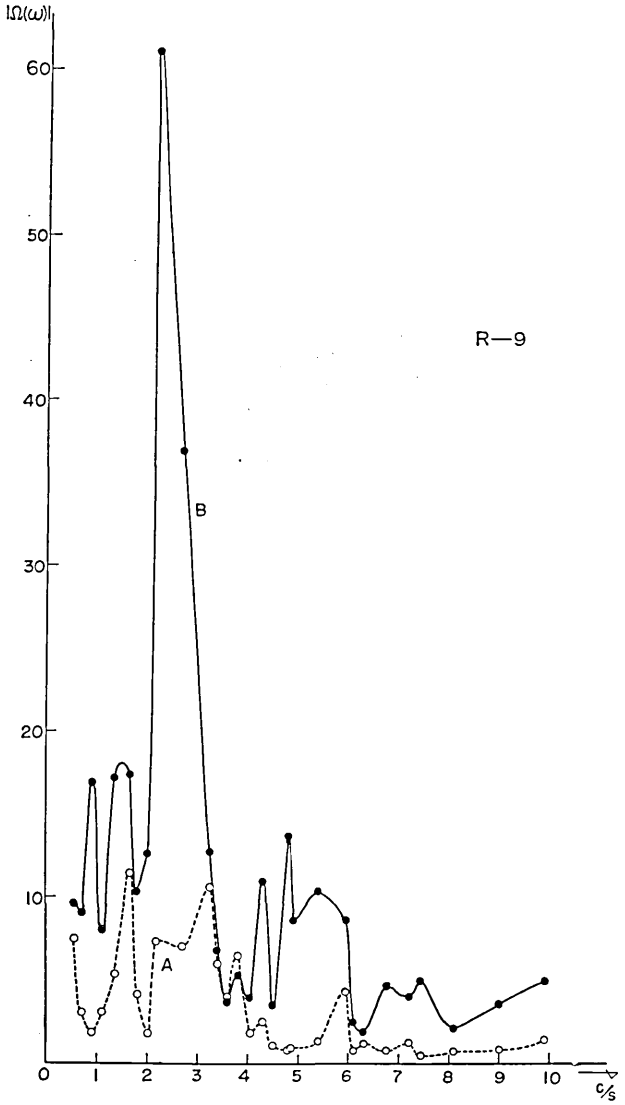

Fig. 29. Spectral density functions of earthquake R—9.

spectral intensity of the surface motion is large, while that of the underground motion is very small. To demonstrate the above-mentioned cases clearly, we made Fig. 39 in which the frequencies of the remarkable intensity of each seismogram are shown. B, C are of the surface and A, D are of the underground. On examining this figure, we came to the conclusion that

i) A similar periodicity exists in both spectra of the surface and underground motions at the frequencies of 0.7~0.9, 1.1~1.8 and 3.2~3.6 cycles per second.

ii) There is another periodicity which appears only on the surface at the frequencies of 2.4~2.7, 4.3~4.7 and 5.4 cycles per second.

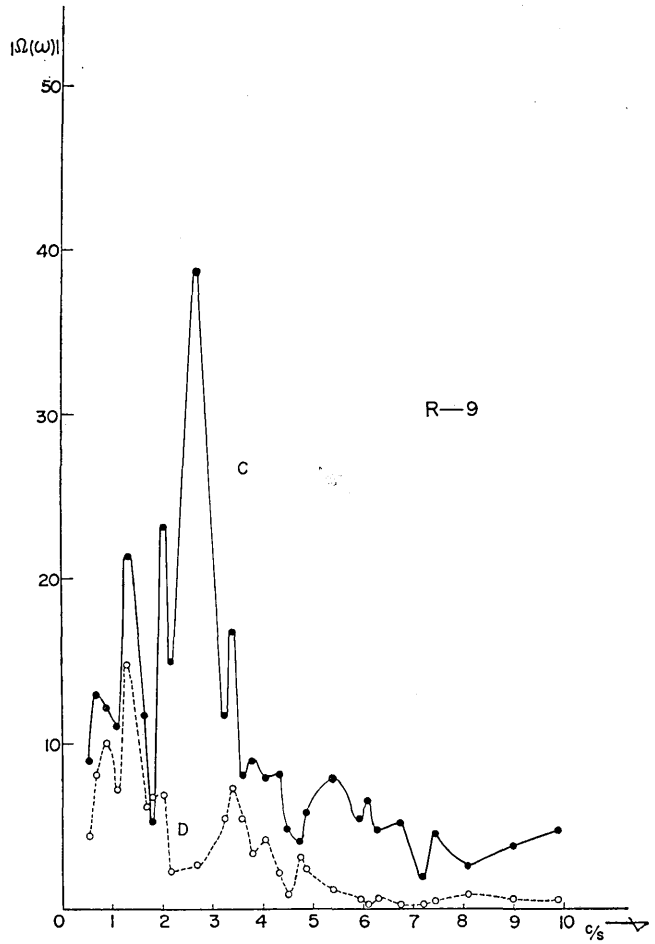

Fig. 30. Spectral density functions of earthquake R—9.

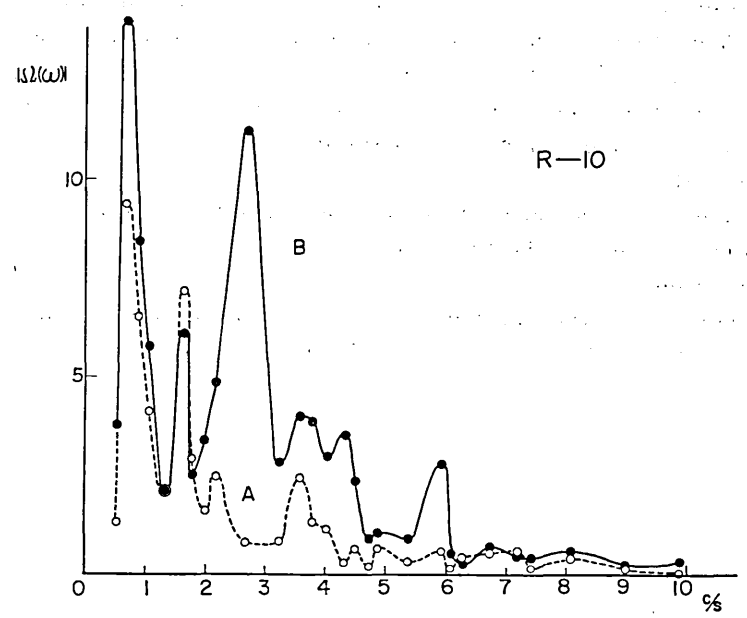

Fig. 31. Spectral density functions of earthquake R—10.

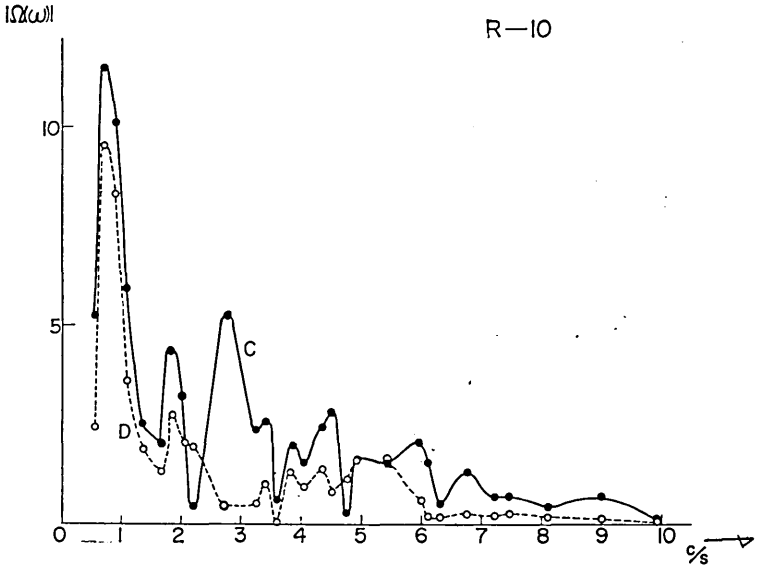

Fig. 32. Spectral density functions of earthquake R—10.

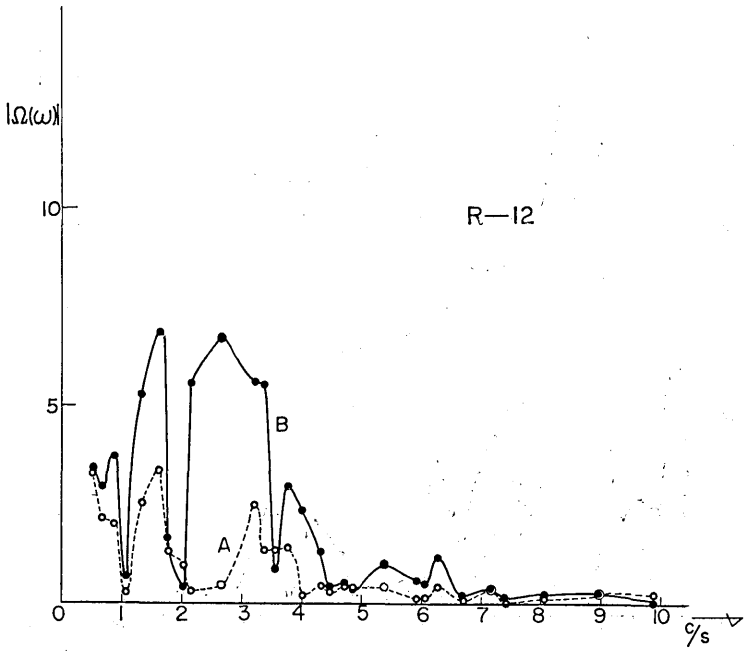

Fig. 33. Spectral density functions of earthquake R—12.

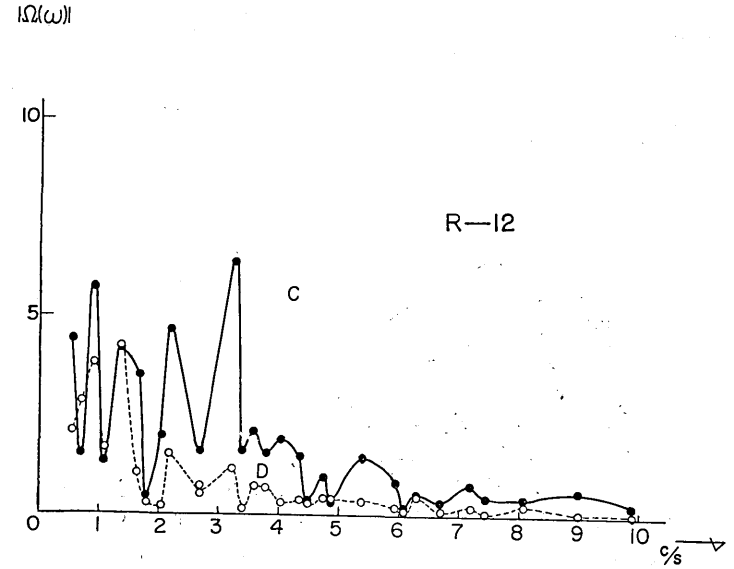

Fig. 34. Spectral density functions of earthquake R—12.

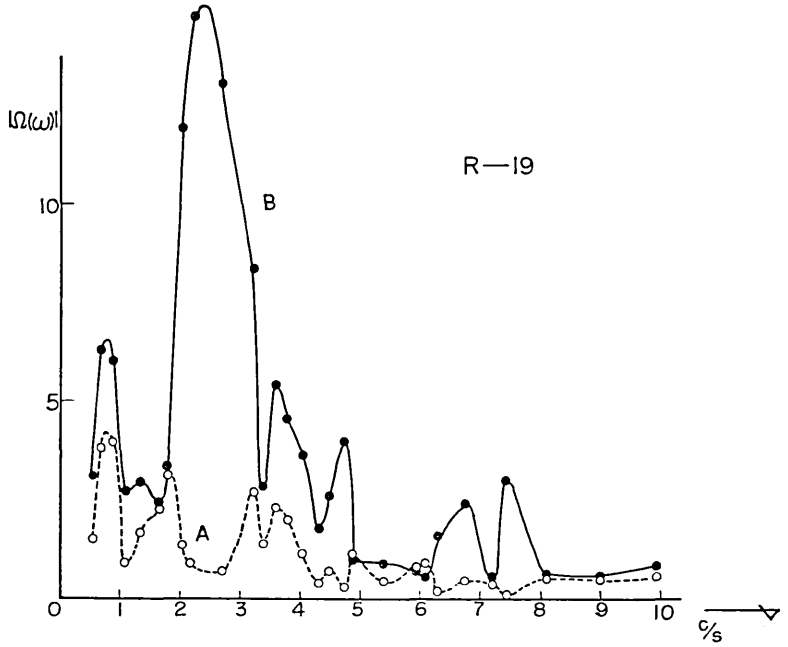

Fig. 35. Spectral density functions of earthquake R—19.

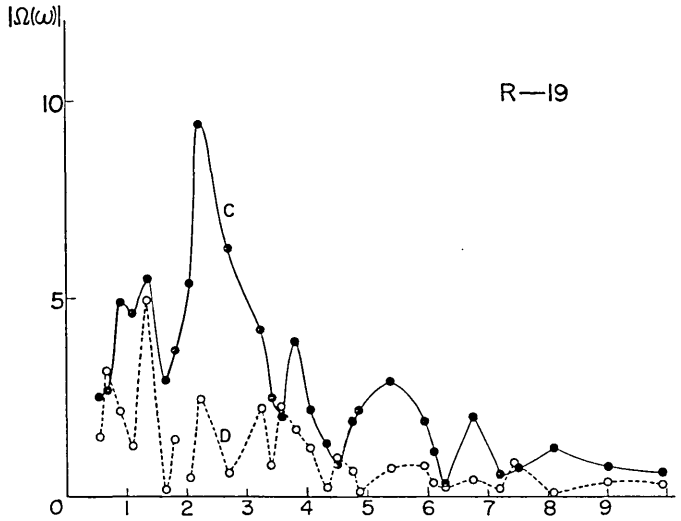

Fig. 36. Spectral density functions of earthquake R—19.

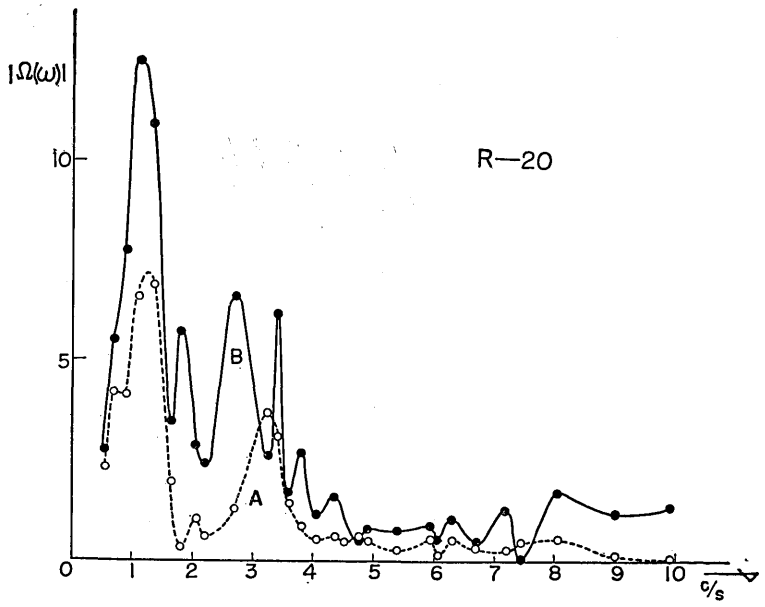

Fig. 37. Spectral density functions of earthquake R—20.

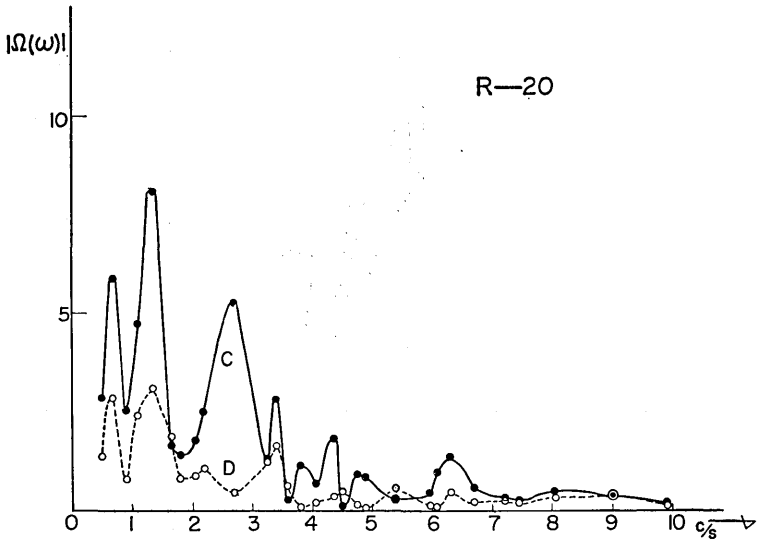

Fig. 38. Spectral density functions of earthquake R—20.

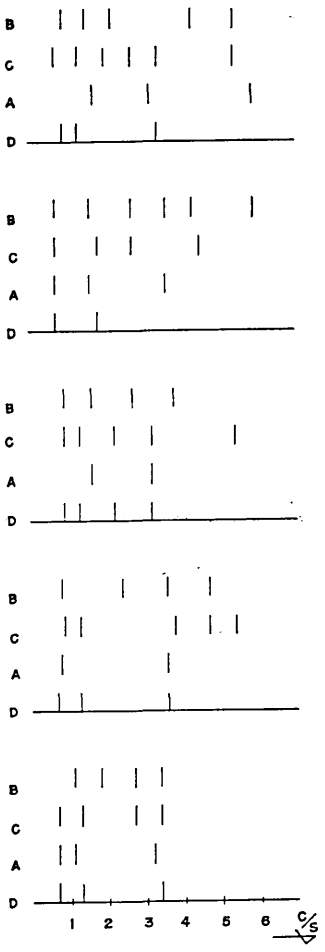

Fig. 39. Frequency of the remarkable intensity in each seismogram.

As to i), it seems that this periodicity is contained originally in the waves of the earthquakes, and as to ii), we can explain the phenomena as follows. As the wave equation in the elastic solid is just the same as that of the signal propagating in the distributed-constant circuit, we may discuss the problem as an electrical analogy. The problem is analogous to the case of a distributed-constant circuit of finite length which is connected to that of infinitesimal length, in which the characteristic impedance differs from that of the former circuit. The receiving end of the circuit is open, and it stands for the ground surface, and the length of line represents the thickness of the stratum.

Now in the finite length distributed-constant circuit, there appears the wave having a frequency of $V/4H$, if the voltage is given at a point on the circuit of infinitesimal length. Here V and H stand for the velocity of the wave and the thickness of the stratum.

Thus we have the loop at the receiving end and the node at the connected point by the following conditions,

$$H=\left(\frac{1}{4}+\frac{n}{2}\right)\lambda \qquad (n=0,\ 1,\ 2\cdots), \tag{39}$$

or

$$f=\frac{2n+1}{4H}V \qquad (n=0,\ 1,\ 2\cdots), \tag{39'}$$

where f and λ are the frequency and the wavelength of the wave respectively. Namely, the amplitude of the surface motion becomes large if the thickness of the stratum satisfies the relation shown in Equation

(39) or (39′), while that of the bottom of the stratum becomes very small.

According to this theory, we can calculate the velocity of shear wave propagating in the stratum that we are now studying, if we have information about the thickness and the predominant period.

Figs. 40 and 41 show the ratios between the spectra of the surface and that of the underground. We cannot find any particular difference between them. So we may conclude that the soil conditions of the two places are almost the same.

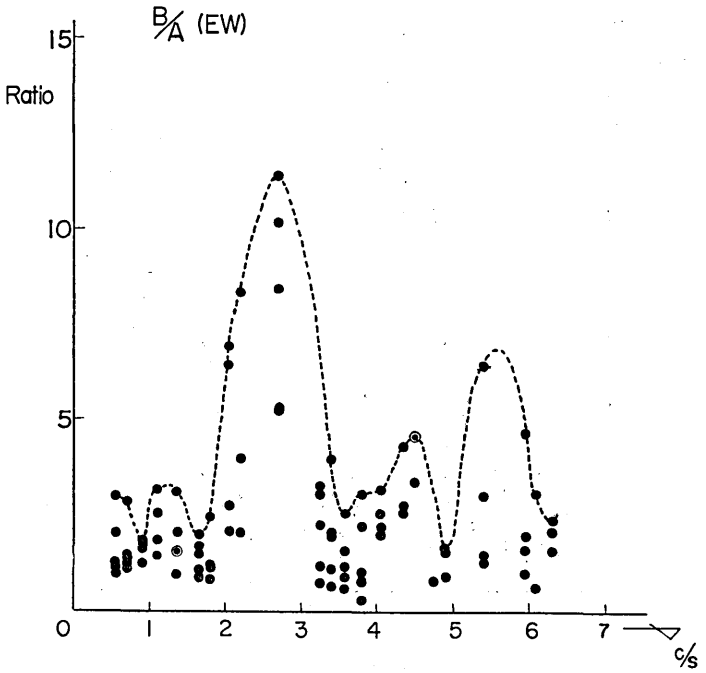

Fig. 40. Ratios between the spectra of the surface and the underground motions. B/A.

From these figures we can see easily the phenomena of resonance at the frequencies of 2.7, 4.5 and 5.5～6 cycles per second. If we assume that the predominant period of 2.7 cycles per second is that of the fundamental wave, the other two cannot be considered as its higher harmonics. We arrive at this conclusion easily from Equation (39). So, some other explanations about them are requested.

Let us now investigate the velocity of shear wave propagating in

the surface stratum. From the data of Saita and Suzuki[46], we calculated the shear wave velocity in the alluvial layer as 100 m/sec, knowing the predominant period to be 0.75 sec and the thickness of the layer to be 18 m. The velocity thus derived is reasonable if we compare it with the values derived by Ishimoto[47] and by the Subsoil Research Team[48]. The observation-point of Saita and Suzuki is covered with a comparatively uniform alluvial formation, called Yurakucho-formation. And this formation is the same as that found in the upper part of our observation-

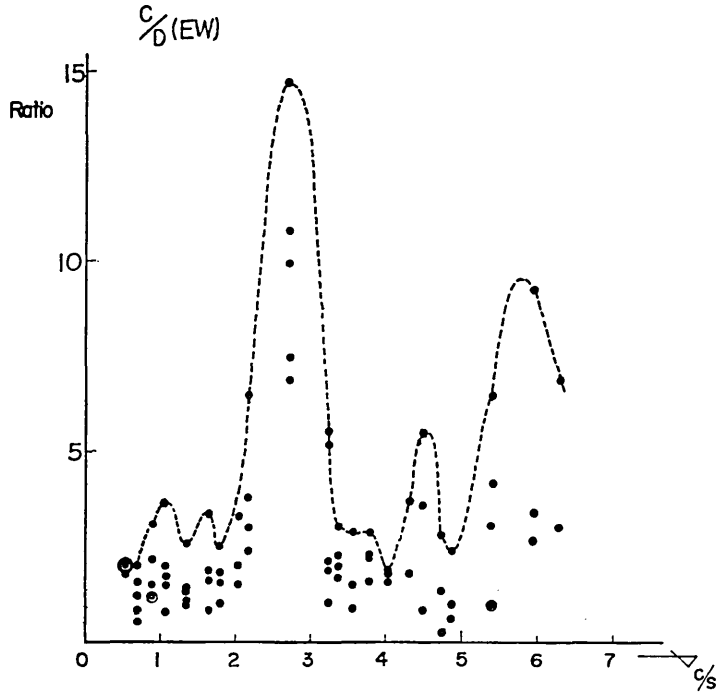

Fig. 41. Ratios between the spectra of the surface and the underground motions. C/D.

points. Using this velocity, we calculated the thickness of the uppermost layer, assuming its predominant period to be 4.5 or 5.7 cycles per second. Then we have 5.6 m or 4.3 m respectively. The former coincide with the results of the boring test.

So we may say that the predominant frequency of the uppermost

46) *loc. cit.*, 15).
47) *loc. cit.*, 14).
48) Subsoil Research Team, *Bull. Earthq. Res. Inst.*, **33** (1955), 471.

layer, Yurakucho-formation, is 4.5 cycles per second. As to the frequency of 5.7 cycles per second, we consider that it is related to the second layer. And if we assume that the predominant frequency of 5.7 cycles per second is due to the multiple reflections of the wave in the second layer, we have 320 m/sec as the shear wave velocity. The above view is verified from another side, without the information of the shear wave velocities, as follows.

It takes $1/2.7\times4=0.093$ sec for the travelling of the wave to travel from the bottom to the surface. And it takes $1/4\times5.7=0.044$ sec and $1/4\times4.5=0.055$ sec to travel through the second and the uppermost layers respectively. The sum of the latter two strongly agrees with the first value.

So we may conclude that the predominant period of 2.7 cycles per second is due to the multiple reflections of the wave between the surface and the Tokyo gravel-bed, and those of 4.5 and 5.7 cycles per second are of the uppermost and the second layer respectively.

7. Theoretical background of the frequency analysis of microtremors

The Fourier series are suitable for analysing periodic functions, and Fourier integrals are apposite in analysing transient phenomena such as earthquake waves. However, natural phenomena are not always included in the above two cases. For example, the waveform of the microtremors cannot be considered as a periodic one, although its power is finite. The above two methods cannot be applied to such a wave. We need more practical theory to analyse it. The theory of generalized harmonic analysis[49] is quite apposite to the case. However, we observe the phenomena in a finite length of the time, so we may say that the analysis of Fourier integrals can be extended to analyse approximately the present phenomena.

For analysis of such complicated waves as microtremors, Ishimoto[50] and Kanai[51]; Aki[52] and Akamatu[53] each devised their own method. The

49) N. WIENER, *The Fourier integral and certain of its applications*, Cambridge, (1933), Chapter 4.
N. WIENER, *Acta Math.*, **55** (1930), 117.
50) *loc. cit.*, 14).
51) *loc. cit.*, 24).
52) *loc. cit.*, 26).
53) *loc. cit.*, 27).

former took up the matter as a problem of zero-crossing, while the latter used the correlation function as their way of analysis.

A theoretical background of the problem of zero-crossing was given by S. O. Rice[54]. This problem has been studied thereafter by many investigators of the communication engineering field[55].

From the view point of physical considerations, the greater part of the intervals of zeros of the output of the narrow band pass filter are given by,

$$\tau_1=\frac{1}{f_b+f_a},$$

where, f_b and f_a are the lower and upper limits of the pass band. Consequently, if we apply this view to an analysis of the microtremors, and assume that the subsoil can be considered as a band pass filter, we could have so-called natural frequency of the subsoil. This is correct, only if the subsoil is considered to be a simple pendulum of low damping. But the characteristics of the seismometer are not considered in the theory, so a careful consideration must be taken into account in applying it to our problem. Concerning Kanai's method we are afraid to say that probably it will miss the high frequency.

Using the method of correlation functions, we are able to analyse waves much more theoretically and accurately than by the period-frequency method. In other words, we consider the power spectrum of the waves in this method, and use convolution integral replacing the periodic expressions used in the case of the Fourier series and that of Fourier integrals.

Now, let us consider the correlation function $\varphi(t)$ derived from $f(t)$, the power of which is finite. If there exists $\Lambda(\omega)$, which is a monotonically increasing function, and if the following expression is valid,

$$\varphi(t)=\int_{-\infty}^{\infty} e^{j\omega t}d\Lambda(\omega), \tag{40}$$

then we can say that $\Lambda(\omega)$ is considered to be the power spectrum of $f(t)$. We assume that $\varphi(t)$ is continuous at $t=0$. Then such $\Lambda(\omega)$ really exists, because it satisfies the necessary conditions of Bochner's theorem.

54) S. O. RICE, *Bell Syst. Techn. J.*, **23** (1944), 282; *ibid.*, **24** (1945), 46; *ibid* **27** (1948), 109.

55) For example, in the book written by J. B. Bendat, explanations of a great number of attractive problems studied by many investigators are given.

J. B. BENDAT, *Principles and Applications of Random Noise Theory*, John Wiley & Sons. Inc., (1958), Chap. 10.

Now from the expression of Stieltjes integrals, if the derivative of $A(\omega)$ exists, we have following Fourier transform pair.

$$\varphi(t)=\int_{-\infty}^{\infty} e^{j\omega t}A'(\omega)d\omega\,, \tag{41}$$

$$A'(\omega)=\frac{1}{2\pi}\int_{-\infty}^{\infty} e^{-j\omega t}\varphi(t)dt\,. \tag{42}$$

So we have the power spectral density function $A'(\omega)$ by the Fourier transform of the correlation functions calculated from the records of microtremors. $A'(\omega)$ is equivalent to $|\Omega(\omega)|^2$, which is derived from the Fourier spectrum of the waves of a finite energy. We must pay attention to the fact that information about the phase is lost completely in this case.

We applied these views to an analysis of the microtremors, and compared the results with those derived from the earthquake observations.

8. Analyses of the microtremors by means of the automatic correlator

From the results of our analyses of numerous seismograms of natural earthquakes, it becomes clear that a special periodic motion proper to the stratum exists. According to Kanai's view[56], the predominant periods of microtremors are almost equal to those of natural earthquakes. Our opinion that subsoil is a kind of filter to seismic waves and microtremors

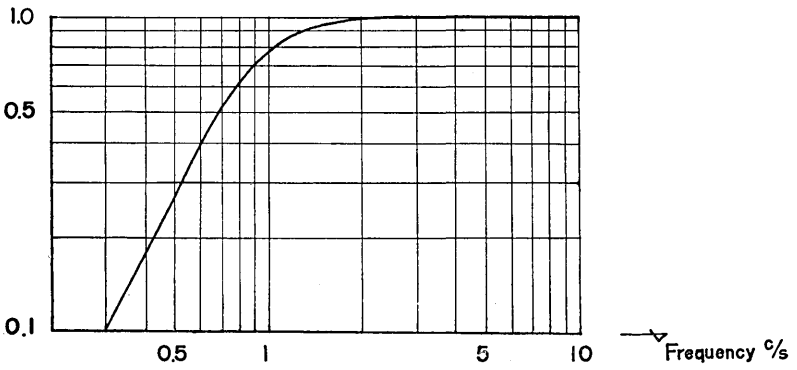

Fig. 42. Response of the seismometer to the constant velocity of varying period of the ground motion.

56) *loc. cit.*, 24).

will now be examined by calculating the correlation function of microtremors on the line we saw in the former section.

The microtremors at the observation-points are almost of a short period caused by traffic noises. So, if we use the usual electromagnetic seismometer to get the input voltage of the correlator, the long period waves will be missed. This is because the output voltage of the usual seismometer is proportional to the ground velocity. We therefore used a moving-coil type electromagnetic seismometer with an integrating circuit. Thus the input voltage of the correlator is proportional to the ground displacement. Fig. 42 is the response of the seismometer to the constant velocity of the ground motion. In Fig. 43 we show the frequency characteristics of the integrating circuit with an amplifier. Fig. 44 is the overall frequency characteristics of the input voltage of the correlator.

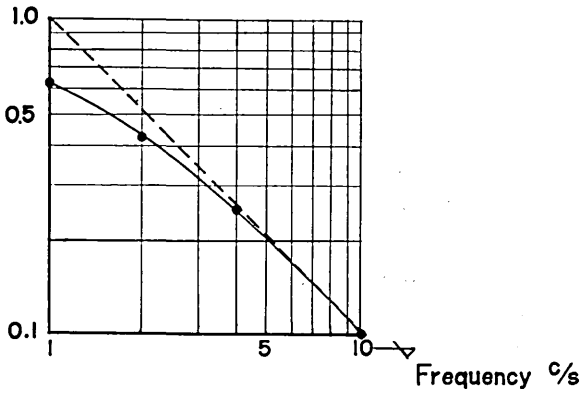

Fig. 43. Frequency characteristics of the integrating circuit with an amplifier.

Here, we will cite the opinions of Aki[57] and Kanai[58] concerning

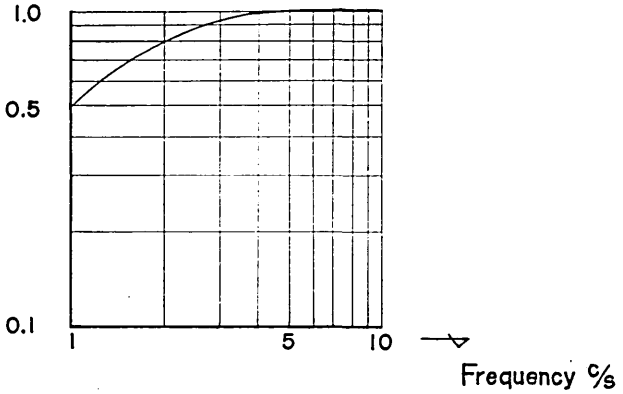

Fig. 44. Overall frequency characteristics of input voltage of the correlator.

57) *loc. cit.*, 26).
58) *loc. cit.*, 24).

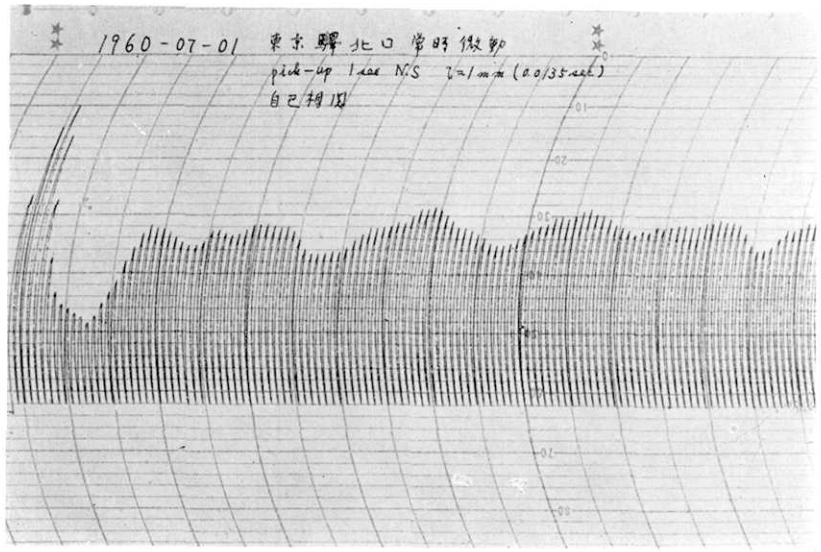
1960-07-01 東京驛北口 常時微動
pick-up 1 sec N-S 1=1 mm (0.0135 sec)
自己相関

Fig. 45.

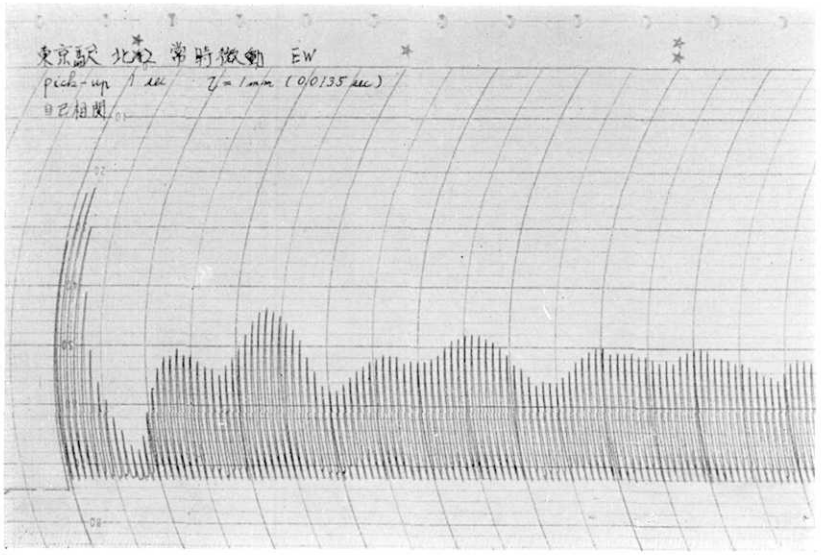
東京駅 北口 常時微動 EW
pick-up 1 sec 1=1 mm (0.0135 sec)
自己相関

Fig. 46.

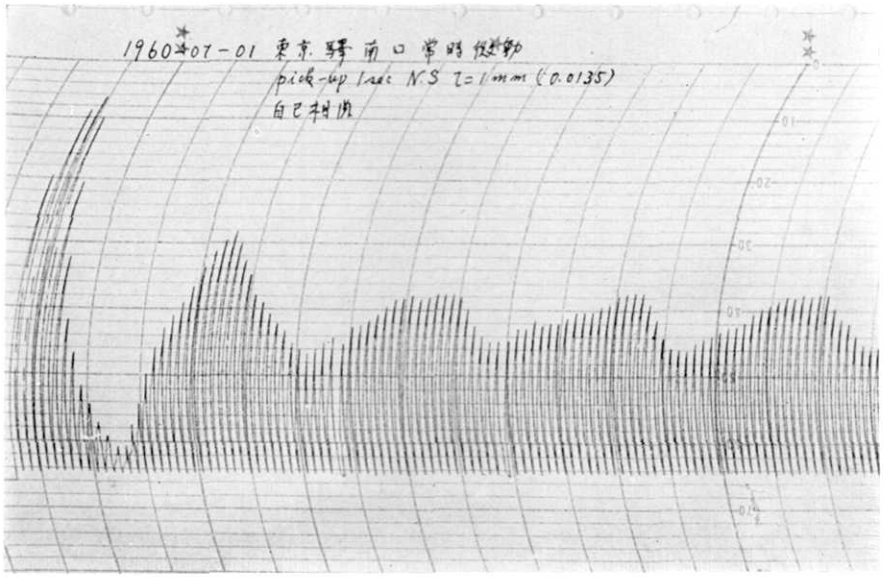
1960-07-01 東京驛南口常時微動
pick-up 1sec N-S 1c=1mm (0.0135)
自己相関

Fig. 47.

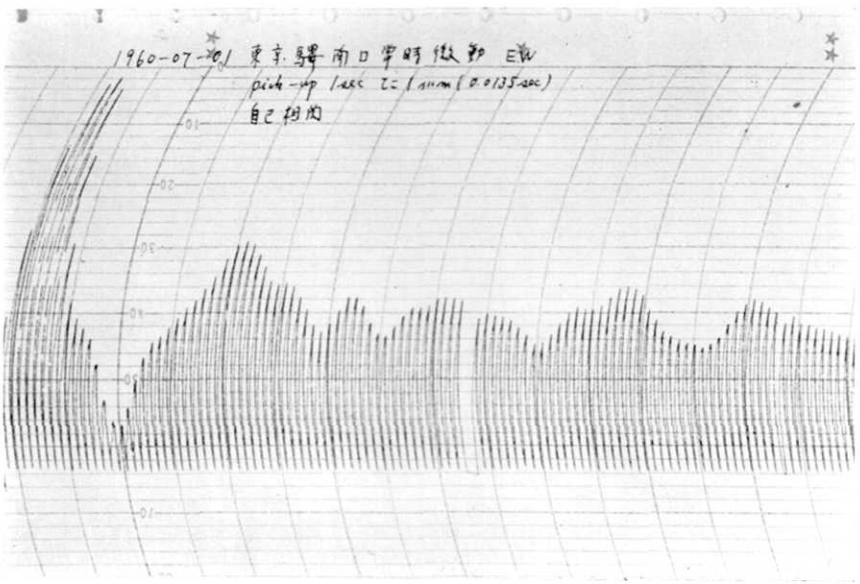
1960-07-01 東京驛南口常時微動 E-W
pick-up 1sec 1c=1mm (0.0135sec)
自己相関

Fig. 48.

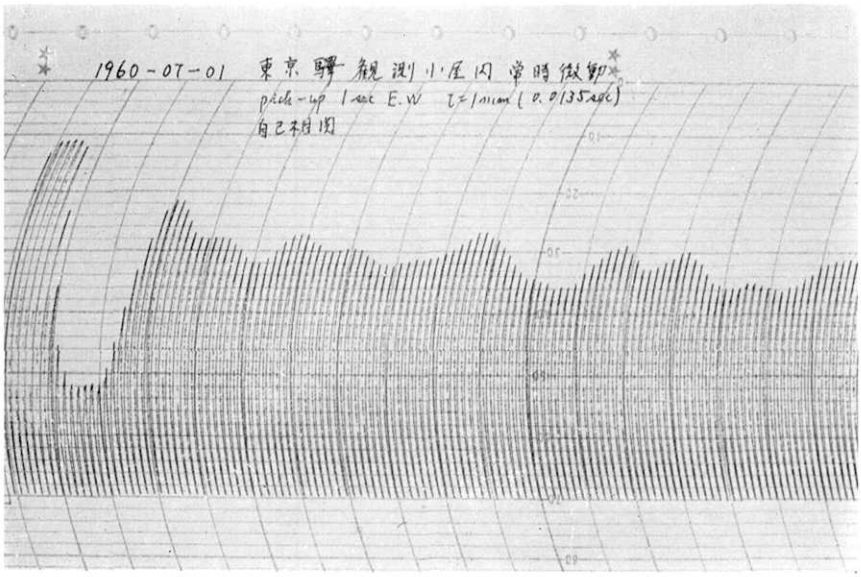
1960-07-01 東京驛 観測小屋内 常時微動
pick-up 1 sec E.W 1cm (0.0135 sec)
自己相関

Fig. 49.

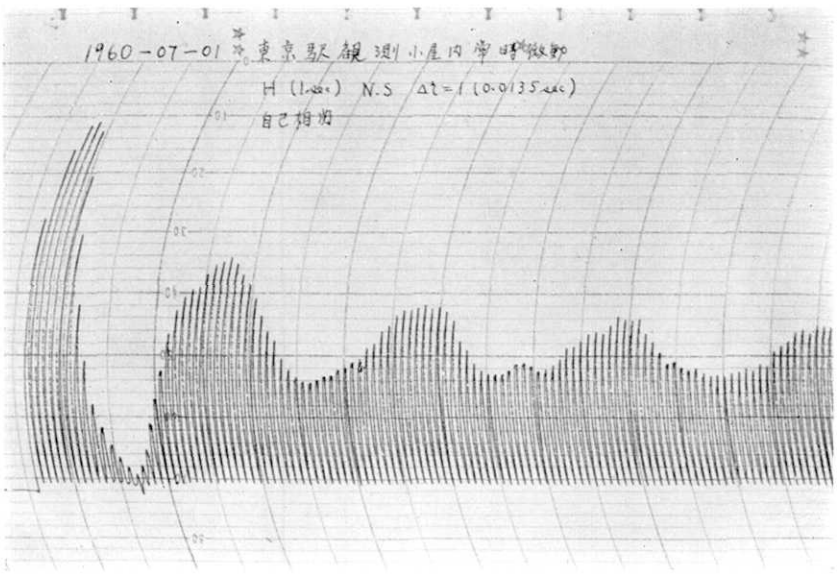
1960-07-01 東京駅 観測小屋内 常時微動
H (1 sec) N.S Δt=1 (0.0135 sec)
自己相関

Fig. 50.

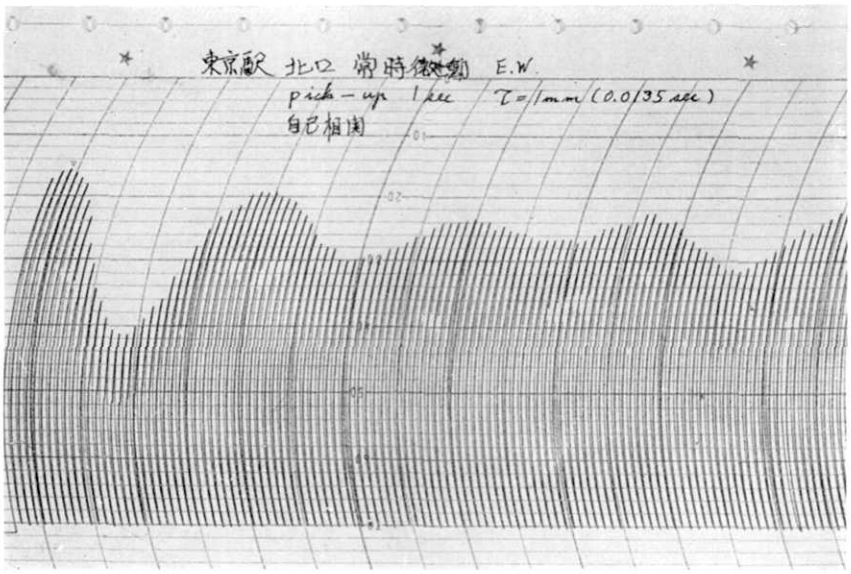
東京駅 北口 常時微動 E.W
pick-up 1 sec τ=1mm (0.0135 sec)
自己相関

Fig. 51.

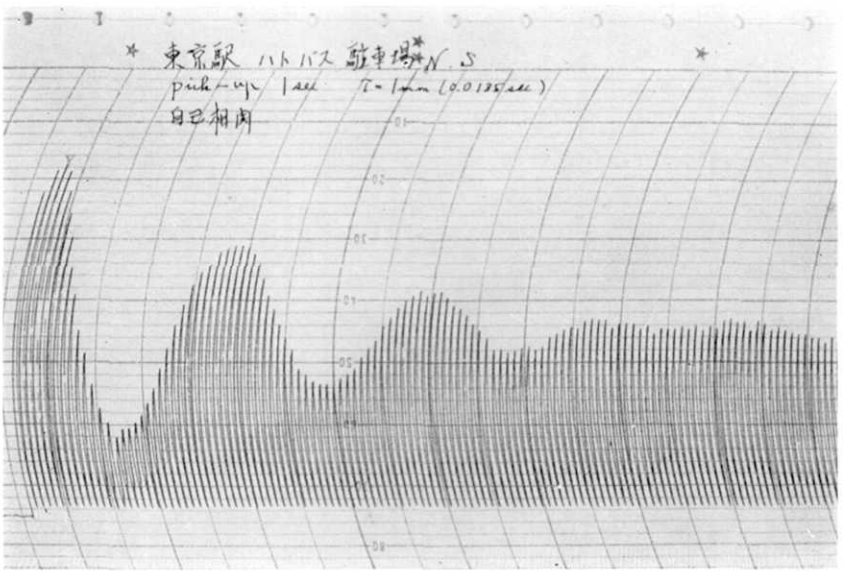
東京駅 ハトバス 駐車場 N S
pick-up 1 sec τ=1mm (0.0135 sec)
自己相関

Fig. 52.

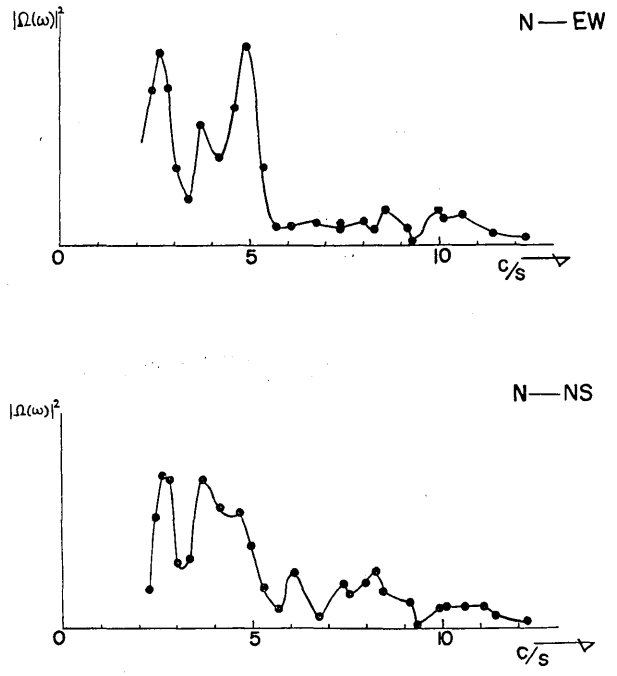

Fig. 53. Power spectral density function calculated from Fig. 45.
Fig. 54. " Fig. 46.

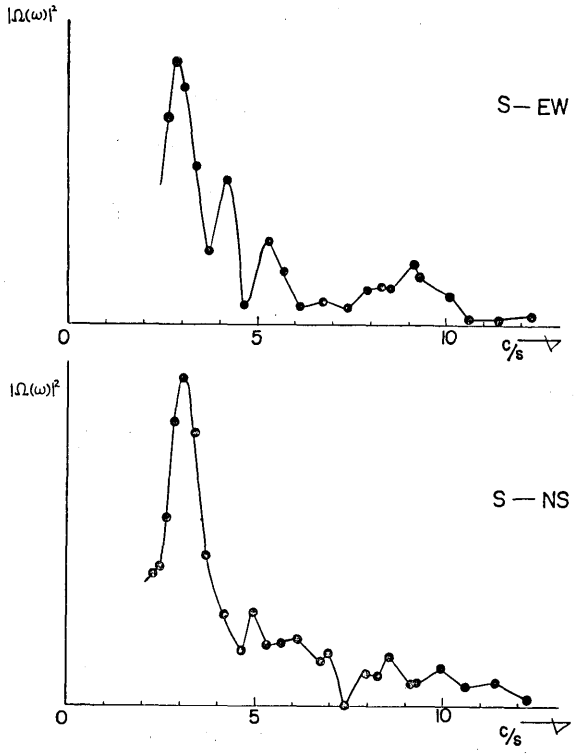

Fig. 55. Power spectral density function calculated from Fig. 47.
Fig. 56. " Fig. 48.

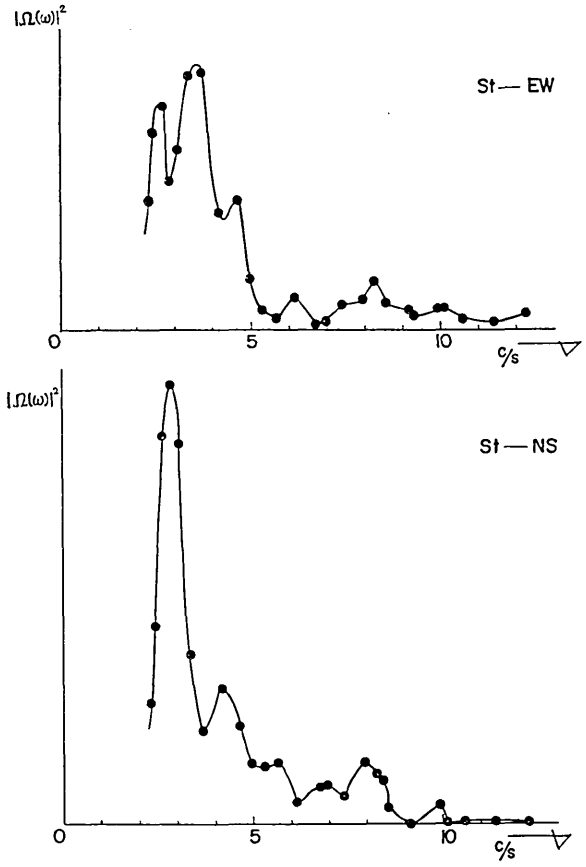

Fig. 57. Power spectral density function calculated from Fig. 49.
Fig. 58. 〃 Fig. 50.

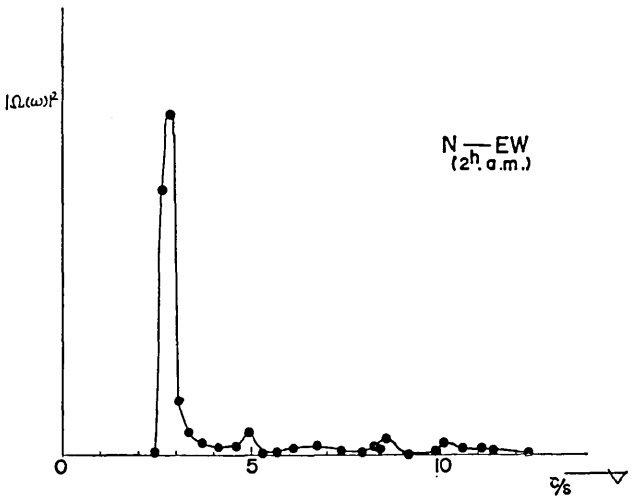

Fig. 59. Power spectral density function calculated from Fig. 51.

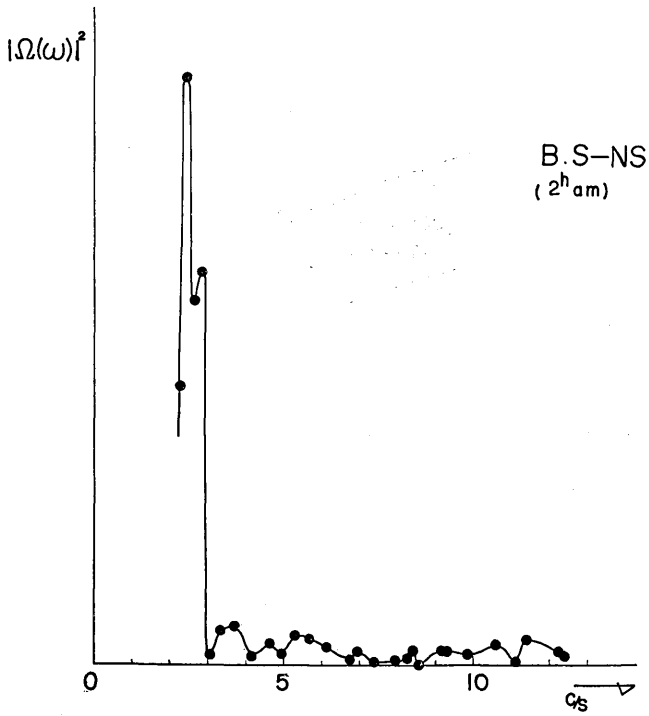

Fig. 60. Power spectral density function calculated from Fig. 52.

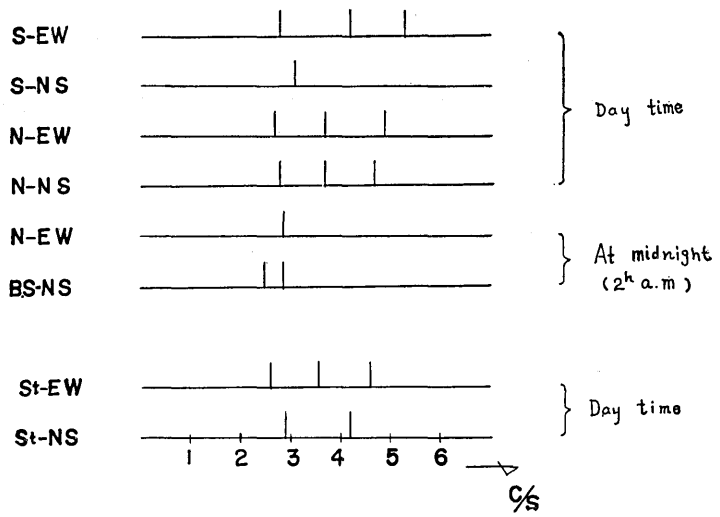

Fig. 61. Frequencies of the remarkable intensities of each power spectral density function.

characteristics of microtremors. Briefly, the former says that the microtremors are a kind of surface wave; and the latter's opinion is that they are bodily waves in a stationary state, while, Akamatu[59] stands neutral between the two opinions. Our opinion is also like Akamatu's. Which seems to be proved by comparing the records obtained in daytime and at midnight—traffic noises are much decreased at night. The calculated auto-correlation functions are shown in Fig. 45 through Fig. 52. And Fourier transforms of these curves, that is power spectral density functions, are shown in Fig. 53 through Fig. 60. The ordinates in these figures are shown in arbitrary scales. The Notations B.S. and St. indicate temporary observation-points at the bus stop and in the attic of the station building, and they are shown in Fig. 18. The input voltage of the correlator at midnight decreases its magnitude by 20 db or more. This shows how the microtremors in daytime are affected by the traffic noises. These results are summarized in Fig. 61. Namely, the frequencies marked with well defined peaks in each figure are arranged in Fig. 61.

Examining Fig. 61, we find that at night there is only a peak, which coincides with those in the spectra of microtremors in daytime and also with the ones derived from the observations of earthquakes. Other predominant frequencies found in the observations in daytime are not always coincident with those found in the earthquake motions. Namely, we can see peaks at 3.7 cycles per second in the spectra of N-EW and N-NS, but not in the spectra of S's. In the case of earthquakes we found the same peak frequency in the spectra of motions both on the surface and underground at the observation-points N and S. (see Fig. 39). So we may conclude that this predominant frequency is not related to the upper layers with which we are concerned, but it may be due to the lower layers or the inherent in the original motions.

Moreover, it is curious that the peak frequencies in the different components of motions are too divergent to be grouped and identified with those appearing in earthquake motions, even if the boundary of the stratum in the ground is inclined or somewhat complicated. So we might conclude that the predominant frequencies shown in Fig. 61 are not related to the strata, except the one near 2.7 cycles per second.

In closing this section, we summarize the results as follows.

i) The forms of the power spectral density functions derived from observations in daytime and at midnight do not resemble each other, and

59) *loc. cit.*, 27).

those derived from observations at midnight are simpler than those in daytime. And because the amplitudes of microtremors are greatly affected by the traffic noises in daytime, it is difficult to ascertain what the predominant frequency of the ground is.

ii) The maximum amplitudes of noises due to traffic are found in the frequency range from 3～6 cycles per second.

iii) To study the frequency characteristics of subsoil, the observations of microtremors at midnight can be used more effectively than observations in daytime.

iv) Microtremors may not always be suitable for indicating the frequency characteristics of the microstructure of subsoils.

v) The predominant periods of microtremors at midnight are equal to those of natural earthquakes.

9. Discussions

In Section 6, we mentioned the results of comparative observations on the surface as well as at the bottom of a bore-hole. The study was successful in gaining a clear knowledge of the frequency characteristics of surface strata than has been so far obtained by investigators. And it has become clear that underground observation is indispensable to the study of the frequency characteristics and other behavior of the stratum. However, it is revealed that the seismograms thus obtained both on the surface and at the bottom of the bore-hole are affected greatly by the multiple reflected waves at each boundary of the surface strata. So the seismograms obtained at the bottom of the bore-hole cannot be considered as the original waveforms of earthquakes. We will now examine in the following, how the original waveforms are changed by the multiple reflections of the waves at the boundaries of the strata. This is our main theme in this paper; and the original waveforms, or the spectrum of earthquake waves may thus be deduced.

First, let us consider the case of a single stratum resting on the surface of the bed-rock. Notations used are as follows:

α_{mn} : Reflection coefficient at the boundary of the m-th and n-th layer.

β_{mn} : Transmission coefficient.

τ : Travel-time of the wave from the boundary to the surface.

$y_{-h}(t)$: Record obtained at the boundary.

$y_o(t)$: Record obtained on the surface.

$f(t)$: Waveforms of the original waves.

Our purpose is to find $f(t)$ from the records of $y_{-h}(t)$ as well as $y_0(t)$. To make the relations between these waveforms clear, we show the schematic figure of time relations between them in Fig. 62.

Referring to Fig. 62, we consider the displacement of the record at $t=t_0$. Then we have the following relations, if the attenuation of the wave is neglected.

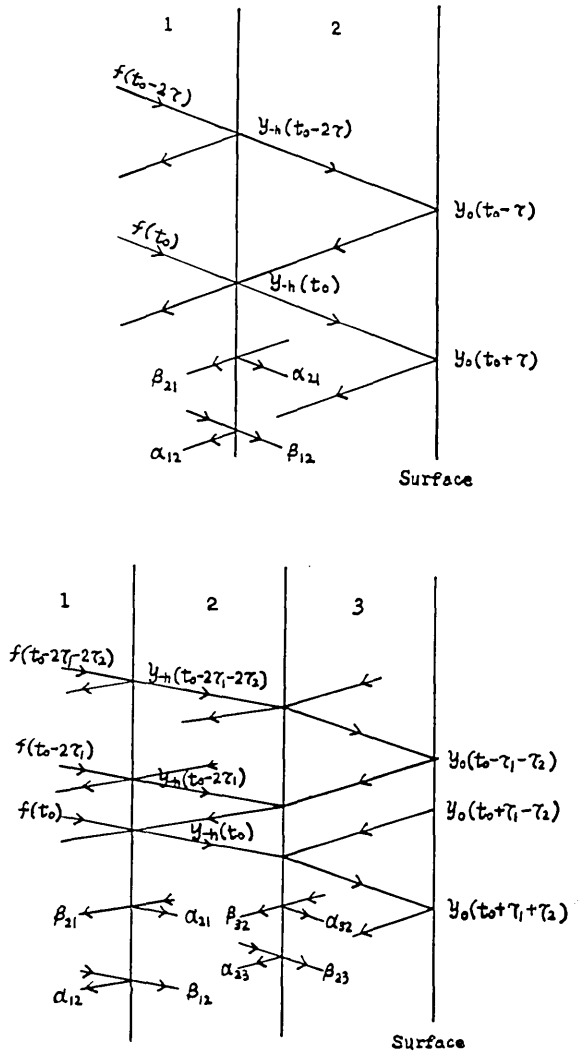

Fig. 62. Schematic figure of time relations among $y_0(t)$, $y_{-h}(t)$ and $f(t)$.

$$\frac{1}{2}y_0(t_0+\tau)=\beta_{12}f(t_0)+\frac{\alpha_{21}}{2}y_0(t_0-\tau)\,, \tag{43a}$$

$$\frac{1}{2}y_0(t_0+\tau)=\beta_{12}f(t_0)+\alpha_{21}y_{-h}(t_0)-\frac{\alpha_{21}}{2}y_0(t_0+\tau)\,, \tag{43b}$$

and,

$$y_{-h}(t_0)=\beta_{12}f(t_0)+\left(\frac{1+\alpha_{21}}{2}\right)y_0(t_0-\tau)\,. \tag{43c}$$

These relations between the amplitudes of waves hold at every instant unless the character of the waves changes.

$$\therefore\quad f(t)=\frac{1}{2(1+\alpha_{12})}\{y_0(t+\tau)+\alpha_{12}y_0(t-\tau)\}\,, \tag{43a'}$$

$$=\frac{1}{(1+\alpha_{12})}\left\{\alpha_{12}y_{-h}(t)+\left(\frac{1-\alpha_{12}}{2}\right)y_0(t+\tau)\right\}\,, \tag{43b'}$$

$$=\frac{1}{(1+\alpha_{12})}\left\{y_{-h}(t)-\left(\frac{1-\alpha_{12}}{2}\right)y_0(t-\tau)\right\}\,, \tag{43c'}$$

$$\because\quad \alpha_{21}=-\alpha_{12},\ \beta_{12}=1+\alpha_{12}\,.$$

So we can calculate $f(t)$ from one of the above relations if τ and α_{12} are known. We have already seen that theoretically speaking, the predominant period is nothing but the time necessary for traveling twice up and down through the stratum. Thus τ can be obtained as one fourth of the fundamental predominant period.

We applied this theory to the actual seismograms, and at $\alpha_{12}=0.6$, we found a comparatively good agreement between the $f(t)$'s as obtained by different formulae, although some discrepancies still remain. These discrepancies are perhaps due to the approximations we made in these calculations. Although we found two strata on the boundary, as we have mentioned, we calculated these waveforms from the equations on the single layer assumption for simplicity. Fig. 63 shows the examples of these calculations. It is remarkable that the complicated waveforms on the surface are simplified by these simple calculations. Moreover, it is to be noted that our idea can be used to separate the surface waves from the shear wave group in complicated seismograms.

If there are two strata overlying the bed-rock, the calculations to determine $f(t)$ become more complicated than before. Referring to Fig. 62 we have,

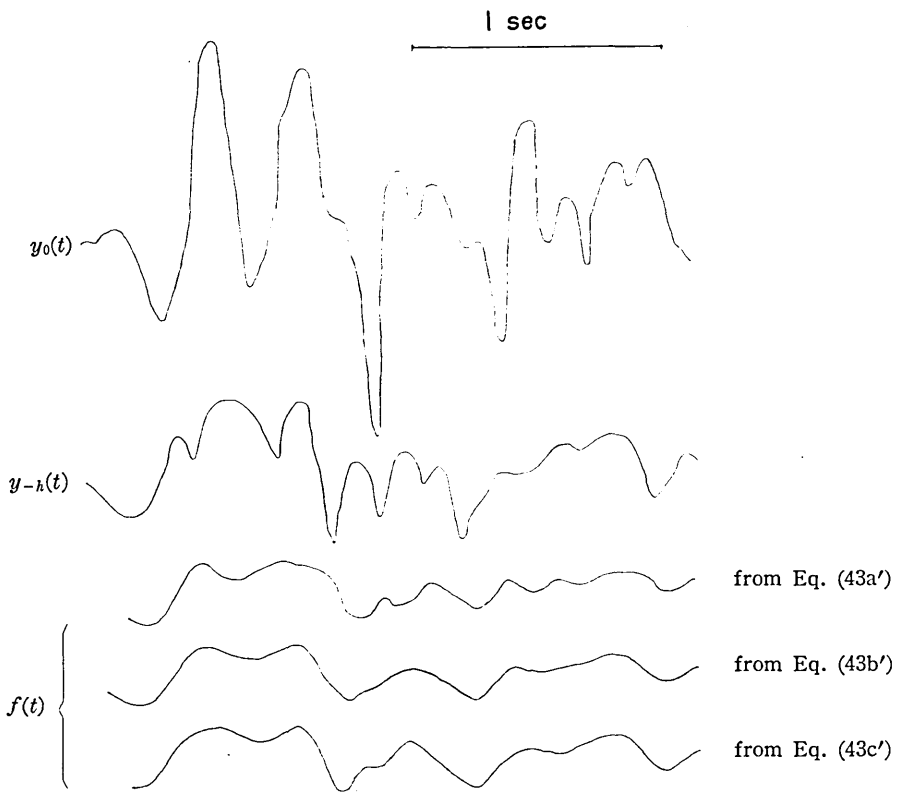

Fig. 63. Examples of calculations (single layer assumption)

$$\frac{1}{2}y_0(t_0+\tau_1+\tau_2)=\frac{\alpha_{32}}{2}y_0(t_0+\tau_1-\tau_2)-\frac{\beta_{32}\alpha_{21}\beta_{23}}{2}y_0(t_0-\tau_1-\tau_2)$$
$$+\frac{\alpha_{23}\alpha_{21}}{2}\{y_0(t_0-\tau_1+\tau_2)+\alpha_{23}y_0(t_0-\tau_1-\tau_2)\}$$
$$+\beta_{12}\beta_{23}f(t_0)\,, \qquad (44a)$$
$$y_{-h}(t_0)=\frac{\alpha_{23}(1+\alpha_{21})}{2\beta_{23}}\{y_0(t_0-\tau_1+\tau_2)+\alpha_{23}y_0(t_0-\tau_1-\tau_2)\}$$
$$+\frac{\beta_{32}(1+\alpha_{21})}{2}y_0(t_0-\tau_1-\tau_2)+\beta_{12}f(t_0)\,, \qquad (44b)$$

.....

etc.

where τ_1 and τ_2 are the travel times of the wave in layers 2 and 3. The above equations are valid at any instant of the time. So we can calculate

$f(t)$ in terms of α from the following equations;

$$f(t)=\frac{1}{2(1+\alpha_{12})(1+\alpha_{23})}\{y_0(t+\tau_1+\tau_2)+\alpha_{23}y_0(t+\tau_1-\tau_2)$$
$$-(1-\alpha_{12})\alpha_{23}y_0(t-\tau_1+\tau_2)-(1-\alpha_{12})y_0(t-\tau_1-\tau_2)\}\ , \quad (44'a)$$

or

$$=\frac{y_{-h}(t)}{(1+\alpha_{12})}-\frac{1-\alpha_{12}}{2(1+\alpha_{12})(1+\alpha_{23})}\{y_0(t-\tau_1-\tau_2)$$
$$+\alpha_{23}y_0(t-\tau_1+\tau_2)\}\ . \quad (44'b)$$

.....

etc.

It is to be remarked that we can determine the value of α_{23} from the ratio between the amplitudes of initial maximums or minimums observed at the boundary of the first and the second layers and on the surface, if $\tau_1>\tau_2$, and only if the initial maximums or minimums are observable within the time $(\tau_1+\tau_2)$ counted from the time of the occurrences of disturbances at the boundary.

We derived the velocity of the shear wave using $\alpha_{12}=0.6$ as 1150 m/sec. The calculation was made under the assumption that the ratio of the densities between the media above and below the top surface of gravel-bed is 1.1.

10. Conclusions

From April of 1960, comparative observations of earthquakes on the surface and at the bottom of bore-holes have been made at two places on the premises of Tokyo Station. Underground seismometers were set at the surface of the gravel-bed. As we set the bore-hole seismometer at the bottom of the bore-hole then proceeded to fill in the hole, the observations must have been made under more nearly natural conditions —that is, in the undisturbed state of the strata—than have been made by former investigators. We calculated the Fourier spectra of the motion during 11 seconds of each seismogram to compare them. The analysed parts of the seismograms are believed to be those of shear waves. We analysed 20 seismograms in total. In addition to these studies, observations of the microtremors were carried out at the same time.

Through the present study, it has become clearer than ever before that the multiple reflections of earthquake waves in the surface strata

give rise to the predominant periods of the strata. Results of the present study are summarized as follows.

i) We found the predominant frequencies of 2.7, 4.5 and 5.7 cycles per second. These are explained by the multiple reflections of the waves which occurred in the strata above the gravel-bed, in the uppermost layer and in the second layer respectively. (see Figs. 40 and 41)

ii) The velocities of the shear wave in the strata are calculated, as being 100 m/sec for the uppermost layer, 320 m/sec for the second layer and 1150 m/sec for the gravel-bed.

iii) From records of the motion on the surface and underground, we calculated the incident waveforms, which it might be possible to observe if the surface strata were removed. (see Fig. 63) The results were successful for explaining that the predominant period is caused by the multiple reflection of the waves. Methods for calculating a single layer case and for the case of a doubly stratified layer are introduced.

iv) These methods are applicable for separating both the surface waves and the shear waves from the complicated seismograms.

v) In every Fourier spectrum of the seismogram analysed, we found the predominant frequency of 0.7～0.9 cycles per second. (see Fig. 39) This frequency may be related to the deeper strata or it might originally have been inherent in the earthquake waves.

vi) The forms of the power spectral density functions derived from the observations of microtremors in daytime and at midnight do not resemble each other; and those derived at midnight (see Figs. 59 and 60) are simpler in their forms than those derived in daytime. (Figs. 53～58) Also the amplitudes of the microtremors are greatly affected by traffic noises in the daytime, which will mask the frequency characteristics of the ground to some extent by their own inherent spectra.

vii) The maximum amplitudes of the noise caused by traffic are found in the frequency range from 3 to 6 cycles per second.

viii) For studying the frequency characteristics of subsoils, the observations of microtremors at midnight can be used more effectively than observations in the daytime, as it is proved in our study that the predominant period of microtremors at midnight is equal to those derived from observations of natural earthquakes.

11. Acknowledgements

The author wishes to express his hearty thanks to Professor Hirosi Kawasumi, for his kind guidance and ceaseless encouragement. The

author's thanks are also due to Messrs. M. Sibano, M. Yanagisawa and Y. Ichinose who kindly helped the author during the course of this study. Lastly the author acknowledges the financial aids of the Japanese National Railways.

---

8. 地表層に依る地震波形の変化

地震研究所　嶋　悦三

地震の発震のからくりとか，magnitude を研究する際には，震源からどの様な波が送り出されたかを知つておかなければならない．今までの研究では，地震の波は伝播の途中では，変形しないということを暗々裡に仮定していたのである．しかしながら，われわれは地盤の違いにより，お互いに非常に近い場所でも，地震の被害の程度がまつたく違うことを経験している．このことから，地震工学の立場からだけでなく，純粋な地震学の立場からも，地震波が伝播の途中どの様な変化をうけるかということを定量的に研究する必要がある．

理論的には，固い第一の物質から軟い第二の物質に地震波が入射する場合，第二の物質が軟かければ軟かい程屈折波の振巾が大きくなることがわかつている．しかしながら，関東大地震の余震を色々な場所で，同じ地震の比較観測をして見ると，振巾比は，必らずしも一定ではなく，これが地震波の周期と関係があることがわかつてきた．

この問題を解釈するために，それは地表層の共振れによるのではないかという説が提出され，理論及び観測面から，研究が推進されてきたが，まだ必らずしもすべての面でこの問題がたしかめられたとはいえない．著者はこの様な地表層における地震波形の変化を，地表と地下における地震動の比較観測からたしかめようとした．この目的のために，特別に地中地震計を設計し，これにより観測を実施した．さらに地震波の解析の他に，地盤の常時微動の解析も行なつた．

この論文は，3部にわかれている．すなわち，第一部では地中地震計についてのべ，第二部では，常時微動を解析するためにつくられた相関計についてのべてある．第三部では，地中地震計によつて得られた，地震記象の解析結果がのべてあり，この結果と，相関計による常時微動の解析結果が比較されている．

次に各々について，その概要をのべる．

1. 地中地震計

地上および地下の地震動の比較観測を行なう場合，井戸とか地下室を利用するのが従前の方法であつた，しかしこの場合，建造物の影響が出ないという保証はまつたくないのである．そこでもし，細い bore-hole の底に適当な電磁式地震計を設置することが出来れば，上記の心配をいくらかでもへらすことが出来るであろう．この様な目的にあう地震計は，われわれの知る限りではまだつくられていなかつた．（但し，周波数帯域の高い地震探鉱の分野では，地中に入れる地震計が相当使用されている．）そのため，われわれは，新しい地震計 (Fig. 2) を設計することにしたのである．

地中に地震計を設置するのであるから，相当乱暴なあつかいにも耐え，またある程度の傾斜にも十分機能を発揮出来るものでなくてはならない．またとつた記録を解析する立場から考えると，変位記象をとつて置いた方が便利なことはいうまでもない．変位記象を得るためには，pendulum には強力な damping をかけて，出力電圧を地動の加速度に比例させ，これを長周期の galvanometer に直結使用すればよいことが電気力学系の analogy から簡単に証明される．この場合この地震計を短周期の galvanometer につなげば加速度記象を得ることが出来る．また傾斜に強いということのために，Willmore suspension を採用した．damping は silicon oil で与えることにした．地震計および galvanometer の常数は，Table 4 および Table 5 に掲げてある．

この様にして作られた地震計が bore-hole の底に設置されるのであるが，地上で前もつて calibration した周波数特性が設置の具合によつてはかわつてしまうかも知れない．そこで，その特性を地上から調べるための簡単な装置を工夫した．これは要するに，地震計に step force をあたえ，この記録すなわち，indicial admittance を Fourier 解析して，観測装置全体の特性を知らうというわけである．この装置による実験結果は，理論値とよくあうことが確かめられた．

この地震計のみの出力感度は 320 μV/gal であり，これを Table 5 に掲げた galvanometer に直結した時の総合倍率は約 80 倍である．変位地震計として使用出来る周波数範囲は 1～20 c/s である．

2. 相　関　計

複雑な波形の中に含まれている information をとりだすのに，相関関数による解析が有効であることはよく知られている．われわれは，この考え方を常時微動の解析に応用するために，自動的に自己または相互相関関数を計算する analog 型相関計を試作した．

Fig. 13 の block diagram に示す様に，入力信号 $f(t)$, $g(t)$ (信号は同じものでもかまわない．その場合は自己相関関数を計算することになる.) は，それぞれ増巾され，パルス巾変調 (P.W.M.) 方式により，(Sampling rate は 120 ヶ/sec) 機構部本体である tape recorder の endless tape に録音される．この場合，録音は，Fig. 14 を見るとわかる様に，head A, B により，それぞれ $f(t)$, $g(t)$ を録音する．すなわち，この tape には 4 ヶの記録が同時に録音されることになる．計算はまず head A から $f(t)$ を，head B から $g(t)$ を再生し，$f(t)g(t)$ の計算を行なう．この掛算は次の様にして行なう．すなわち，一方は low pass filter を通して復調し，一方は，P.W.M. signal のままとり出し，これで復調した方の signal を chop して，巾，高さとも変調された矩形波にし，これを low pass filter に通す．そしてその出力電流で condenser を充電すれば，それが $\int f(t)\cdot g(t)dt$ となる．

この計算が終ると，condenser の両端子は一定電圧に clamp されて，次の計算にそなえる．次に $g(t+\tau)$ をつくるわけであるが，これは，Fig. 14 に示す guide roller が一つの計算終了と同時に自動的にきめられた長さだけ滑り下り，head A と head B 間にはいる tape の長さを伸ばすことによりなされる．この様にして，次々に計算が自動的におこなわれ，きまつた遅延時間までの計算をしおわると，相関計は自動的に全電源が切れ停止する．なお condenser の電圧は penwriter で記録される．なお endless tape におさめられる記録は約 40 sec であり，τ は 0.00675 sec, 0.0135 sec, 0.0270 sec の 3 ヶのうちどれか一つをえらぶことが出来る．とり得る最大遅延時間は約 5 sec である．一計算 cycle に要する時間は 7.5 sec 程度である．

3. 地盤の振動性状

1960 年の 4 月から東京駅構内において，地上と地下の地震動の比較観測を行なつている．地下の地震計は東京礫層の上面に設置されてあり，これを設置するために掘つた細いボーリング孔は埋めもどしてある．したがつて，われわれの観測は非常に自然に近い状態で行なわれているといつてよかろう．とれた地震記録 20 の主要動 (S 波と思われる) の部分 11 秒間について Fourier 解析を行ない，さらにこの結果と比較するために，常時微動の観測が行なわれた．

この研究により，土地の卓越周期が，地盤内における地震波の重複反射に起因するということが前より一層はつきりした．結果をまとめると次の様になる，

i) 東京駅附近においては，2.7 c/s, 4.5 c/s, 5.7 c/s の卓越震動があり，これらは，礫層上部の二つの層内に起つた重複反射によるものとして都合よく説明できる．(Fig. 40, Fig. 41)

ii) 第一層および第二層の S 波の伝播速度は，それぞれ，100 m/sec, 320 m/sec となり，また礫層内の速度は 1150 m/sec となる．

iii) 地上と地下の記録から，表面層がない時に観測されるであろう波形を計算した．(Fig. 63) この結果は，卓越周期が，表面層の重複反射によることの証明になると考えられる．こういう計算をする場合の便利のために，表面に一層および二層ある場合についての波形の式を求めておいた．

iv) この方法は，地震記象から，S 波と表面波を分離するのに役立つと思われる．

v) どの地震の Fourier spectrum にも 0.7～0.9 c/s 附近に卓越した波が見られる．(Fig. 39) こ

れはさらに深い地盤に起因しているかも知れない．また地震波にもとから含まれていたのかも知れない．

vi) 常時微動の power spectral density function は，昼間と夜中にとつたものとではお互いに似ていない．夜中にとつたものは昼間にとつたものに較べて形が簡単である．(Fig. 59, Fig. 60) このことは昼間の常時微動が近くの交通機関による noise の影響を非常にうけるためであると考えられる．

vii) 交通機関による noise は 3～6 c/s が大きい様である．

viii) 夜中に観測した常時微動の power spectral density が max. になる微動の周期は，地震観測から得られた卓越周期と一致する．このことから，常時微動から卓越周期を知るには，日中よりも夜間の観測の方が効果的であるといつてよかろう．